# Numerical simulation of a kinetic model for chemotaxis

Nicolas Vauchelet

# Numerical simulation of a kinetic model for chemotaxis.

N. Vauchelet

UPMC, Univ Paris 06, UMR 7598 LJLL, Paris F-75005 France ;
CNRS, UMR 7598 LJLL, Paris, F-75005 France,
and INRIA Projet BANG,
Tel.: (+33)(0)1 44 27 37 72 Fax: (+33)(0)1 44 27 72 00

*E-mail addresses:* vauchelet@ann.jussieu.fr

**Abstract**

This paper is devoted to numerical simulations of a kinetic model describing chemotaxis. This kinetic framework has been investigated since the 80's when experimental observations have shown that the motion of bacteria is due to the alternance of 'runs and tumbles'. Since parabolic and hyperbolic models do not take into account the microscopic movement of individual cells, kinetic models have become of a great interest. Dolak and Schmeiser (2005) have then proposed a kinetic model describing the motion of bacteria responding to temporal gradients of chemoattractants along their paths. An existence result for this system is provided and a numerical scheme relying on a semi-Lagrangian method is presented and analyzed. An implementation of this scheme allows to obtain numerical simulations of the model and observe blow-up patterns that differ greatly from the case of Keller-Segel type of models.

**Keywords.** Chemotaxis; Kinetic equations; semi-Lagrangian method; convergence analysis.

**AMS subject classifications:** 92C17; 92B05; 65M12; 82C80.

## 1 Introduction and modelling

Chemotaxis is the phenomenon in which cells direct their movements according to certain chemicals in their environment. A possible issue of a positive chemotactical movement is the aggregation of organisms involved to form a more complex organism or body. Many attempts for describing chemotaxis from a Partial Differential Equations viewpoint, i.e. for a large population, have been considered. At the macroscopic level the most famous is the Patlak, Keller and Segel model [28, 34]. Although this models have been successfully used to describe aggregation of the population (see [25, 26, 41] for surveys), these macroscopic models have several shortcomings, for instance they do not take into account the detailed individual movement of cells.

Therefore another approach involving kinetic equations to describe chemotaxis has been proposed. The so-called Othmer-Dunbar-Alt system [31, 33, 35] governs the evolution of the

distribution function $f$ of bacteria at time $t$, position $x \in \omega$ and velocity $v \in \mathcal{V}$ and of the concentration of chemoattractant $S$. The system writes in the following way :

$$\begin{cases} \partial_t f + v \cdot \nabla_x f = \displaystyle\int_{v' \in \mathcal{V}} (T[S](v' \to v) f(v') - T[S](v \to v') f(v))\, dv', \\ -\Delta S + S = \rho(t,x) := \displaystyle\int_{v \in \mathcal{V}} f(t,x,v)\, dv, \end{cases} \tag{1.1}$$

completed with the initial condition

$$f(0,x,v) = f^0(x,v). \tag{1.2}$$

The turning kernel $T[S](v' \to v)$ denotes the rate of cells changing their velocity from $v'$ to $v$.

This system models the evolution of flagellated bacteria such as E. Coli. It has been observed that a bacterium moves along straight lines, suddenly stop to choose a new direction and then continue moving in the new direction until the cells receptors saturate. The movement of the bacterium is then due to the alternance of these 'run' and 'tumble' phases [1, 40]. Cells are able to compare the present chemical concentrations to previous ones and thus to respond to temporal gradients along their paths. The decision to change direction and turn or to continue moving depends then on the concentration profile of the chemical $S$ along the trajectories of cells and detailed models have been proposed in [18, 19, 16]. In [16] the authors propose to consider simply a turning kernel of the form :

$$T[S](v' \to v) = \phi(\partial_t S + v' \cdot \nabla_x S). \tag{1.3}$$

The rate of turning is greater if the gradient concentration along the trajectory $\partial_t S + v \cdot \nabla_x S$ is negative than when it is positive. Experimentally, in the absence of gradients of concentration, an individual cell of E. Coli performs a random walk with a mean duration of run times of $1s$ (see [30]). Due to the influence of the chemoattractant a cell sensing a positive gradient of concentration has a run 4 times longer. Then, in this simplified model, we consider that $\phi$ is a positive nonincreasing smooth function; more precisely,

$$\phi \in C^\infty(\mathbb{R}), \quad \phi' < 0, \quad \phi(z) = \begin{cases} 1 & \text{if } z < -\alpha, \\ 1/4 & \text{if } z > \alpha, \end{cases} \tag{1.4}$$

for a given positive $\alpha$ small.

In this work, we are interested in the evolution of the bacteria concentration in a Petri box, which is approximated by a bounded domain $\omega \subset \mathbb{R}^2$. The velocity of bacteria has a constant modulus $V$, therefore we take $\mathcal{V} = \mathbb{S}_V := \{v \in \mathbb{R}^2 \text{ with } \|v\| = V\}$. We denote $\Omega = \omega \times \mathcal{V}$. The system can be then rewritten in the following way :

$$\begin{cases} \partial_t f + v \cdot \nabla_x f = \displaystyle\int_{v' \in \mathcal{V}} \phi(\partial_t S + v' \nabla_x S) f(v')\, dv' - 2\pi \phi(\partial_t S + v \nabla_x S) f(v), \\ f(0,x,v) = f^0(x,v), \\ -\Delta S + S = \rho(t,x) := \displaystyle\int_{v \in \mathcal{V}} f(t,x,v)\, dv, \end{cases} \tag{1.5}$$

This system is completed with the specular reflection conditions

$$f(t,x,v) = f(t,x,v - 2(v \cdot \nu)\nu), \quad \forall\, x \in \partial\omega,\ v \in \mathcal{V} \text{ such that } v \cdot \nu(x) > 0, \tag{1.6}$$

where $\nu(x)$ is the outward unit vector at the point $x$ of the boundary $\partial\omega$. And for the chemoattractant concentration, we set Neumann boundary conditions :

$$\partial_\nu S(t,x) = 0, \quad \forall\, x \in \partial\omega. \tag{1.7}$$

This system is composed of a kinetic equation coupled to an elliptic equation. Therefore we propose in this work to use techniques which have proven their efficiency for the numerical resolution of the Vlasov-Poisson system in plasma physics to deal with the numerical approach of system (1.5). Lagrangian methods like Particle-In-Cell methods which consist of approximating the plasma by a finite number of macro-particles are usually performed for the Vlasov equation (see [4]). However, these methods are known to be very useful for large scale problems but are very noisy and do poor job on the tail of the distribution function. To remedy this problem, Eulerian methods have been proposed. They consist of discretizing the Vlasov equation on a mesh of phase space. Among them, finite volume schemes are known to be robust and computationally cheap [9, 12, 14, 22] but very constrained by a CFL condition. Semi-Lagrangian methods are other kinds of Eulerian method allowing to obtain accurate description of the distribution function [39, 2, 3, 15]. They consist of directly computing the distribution function at each time step on a fixed Cartesian mesh of the phase space by following the characteristics curves backward and interpolating the value at the base of the characteristics. We refer to [23] for a review on Eulerian methods. Then, we will use in this work a semi-Lagrangian method for the numerical resolution of model (1.5).

The paper is organized as follows. In the next section we state and prove an existence and uniqueness result for the system (1.5)–(1.7). For the sake of simplicity this study is considered in the whole domain $\mathbb{R}^2$, which allows to have an explicit expression of $S$ thanks to the Bessel potential. Section 3 is devoted to the numerical resolution of this system. We first recall the semi-Lagrangian method used for the discretization of the kinetic transport equation. Then we present the algorithm of resolution of the whole system (1.5). Finally, an analysis of this scheme under additional assumptions furnishes a convergence result in $L^2$ of the discrete approximation towards the solution of model (1.5). Numerical simulations, which shows the aggregation phenomenon observed for bacteria E. Coli, are presented and discussed in comparison to those for Keller-Segel in section 4.

# 2 Existence result

For the sake of simplicity, we consider in this section that $\omega = \mathbb{R}^2$ and $\Omega = \mathbb{R}^2 \times \mathcal{V}$.

The existence of solutions to kinetic models of chemotaxis has been investigated in several papers. In [11, 27], global existence for the initial value problem (1.1) in $\mathbb{R}^3$ and in $\mathbb{R}^2$ has been obtained under the assumption that the turning kernel is controlled by terms involving $S(t, x+v)$ and $S(t, x-v')$. Dispersive methods are used to obtain a priori estimates. These results has been extended in [8] for more general assumptions on the turning kernel. All these papers took into account the effect of the gradient of the chemical signal and showed global existence of solutions. However, these rigorous global existence results have not included the temporal derivative of the signal in the growth condition of the turning frequency. In ref. [17], the authors investigate global existence of solutions (not necessary unique) for general hyperbolic chemotaxis models where the turning kernel takes into account the temporal derivative of the chemoattractant through the evolution of internal states but only in the one-dimensional physical space.

For the sake of completeness of this paper, we propose here to extend these results to model (1.5) considered in the whole domain $\Omega = \mathbb{R}^2 \times \mathcal{V}$ and to establish existence and uniqueness of global-in-time solution. The main novelty is due to the dependance of the cross-section of the turning operator on the time derivative of the chemoattractant concentration. We use the following expression for the chemoattractant concentration :

$$S(t,x) = (G * \rho(t))(x), \qquad \text{where} \quad G(x) = \frac{1}{4\pi}\int_0^\infty e^{-\pi\frac{|x|^2}{4s} - \frac{s}{4\pi}}\frac{ds}{s}.$$

The function $G$ is known as the Bessel potential. The idea to overcome the difficulty raised by the term $\partial_t S$ in the turning kernel expression (1.3) is to use the conservation of the density :

$$\partial_t \rho + \nabla_x \cdot J = 0, \qquad J(t,x) = \int_{\mathcal{V}} v f(t,x,v)\, dv. \tag{2.1}$$

We have then

$$\partial_t S = G * \partial_t \rho = -G * \nabla_x \cdot J = -\nabla_x G * J, \tag{2.2}$$

where the convolution between two vectors is defined by $\nabla_x G * J = \partial_{x_1} G * J_1 + \partial_{x_2} G * J_2$. It implies a control on the partial derivatives of $S$ with respect to time thanks to controls on $J$ (see [7]). We can then rewrite the problem (1.5) as

$$\begin{cases} \partial_t f + v \cdot \nabla_x f = \displaystyle\int_{v' \in \mathcal{V}} \phi(\nabla_x G * (v'\rho - J)) f(v')\, dv' - 2\pi\phi(\nabla_x G * (v\rho - J)) f(v), \\ f(0,x,v) = f^0(x,v), \end{cases} \tag{2.3}$$

We first define the notion of weak solutions for (2.3) on $(0,T)\times\Omega$.

**Definition 2.1** *We say that $f$ is a weak solution of (2.3) on $L^q(0,t_0;L^p(\Omega))$ for $t_0 > 0$ and $p,q \geq 1$, if for any test function $\psi \in \mathcal{D}([0,t_0)\times\Omega)$, we have*

$$\begin{aligned} \int_{(0,t_0)\times\Omega} (\partial_t\psi + v\cdot\nabla_x\psi) f\, dxdvdt = &- \int_{(0,t_0)\times\Omega}\int_{\mathcal{V}} \phi(\nabla_x G * (v'\rho - J)) f(v')\psi\, dtdxdvdv' \\ &+ 2\pi \int_{(0,t_0)\times\Omega} \phi(\nabla_x G * (v\rho - J)) f\psi\, dtdxdv + \int_\Omega f^0(x,v)\psi(0,x,v)\, dxdv, \end{aligned}$$

*where the cells density $\rho$ and the current density $J$ are defined by*

$$\rho(t,x) = \int_{\mathcal{V}} f(t,x,v)\, dv, \quad J(t,x) = \int_{\mathcal{V}} v f(t,x,v)\, dv. \tag{2.4}$$

We state the following existence and uniqueness result :

**Theorem 2.2** *Assume $f^0 \in L^1_+ \cap L^\infty(\Omega)$ and that the turning kernel $T$ is defined by (1.3)–(1.4). Then the initial value problem (2.3) admits a unique global weak solution $f$ satisfying $f \in L^\infty((0,\infty); L^1_+ \cap L^\infty(\Omega))$.*

*Moreover, if $f^0 \in W^{2,2}(\Omega) \cap W^{1,\infty}(\Omega)$ then for all $t_0 > 0$, there exists a constant $C_0$ depending on $t_0$ and on the data such that the weak solution of (2.3) satisfies*

$$\|f\|_{L^\infty((0,t_0);W^{2,2}(\Omega)\cap W^{1,\infty}(\Omega))} \leq C_0\,; \qquad \text{and} \qquad \|\partial_t f\|_{L^\infty((0,t_0);L^\infty(\Omega))} \leq C_0.$$

The proof of this result is split into two steps. First, we prove the local-in-time existence of a unique solution. The smoothness assumption (1.4) on $\phi$ provides thanks to a fixed point procedure the uniqueness of solution. Then, thanks to a priori estimates, we extend this solution up to $t_0$ for all $t_0 > 0$ and then recover global existence. The main tool in the proof of Theorem 2.2 is an a priori estimate given in the following Lemma :

**Lemma 2.3** *Let $t_0 > 0$ and $f^0 \in L^\infty(\Omega)$. Let $f$ be a weak solution of (2.3), such that $f \in L^1((0,t_0), L^1_+ \cap L^\infty(\Omega))$. Then we have for a.e. $t \in (0,t_0)$, $\|f(t,\cdot,\cdot)\|_{L^1(\Omega)} = \|f^0\|_{L^1(\Omega)}$ and*

$$\|f\|_{L^\infty((0,t_0);L^\infty(\Omega))} \leq C(\|f^0\|_{L^\infty(\Omega)})\, e^{2\pi t},$$

*where the constant $C(\|f^0\|_{L^\infty(\Omega)})$ depends only on the initial data.*

**Proof.** First the conservation of the mass shows that

$$\|f(t,\cdot,\cdot)\|_{L^1(\Omega)} = \|f^0\|_{L^1(\Omega)}.$$

From the bound $1/4 \leq \phi \leq 1$ of $\phi$ (1.4) we deduce

$$\partial_t f(t,x,v) + v \cdot \nabla_x f(t,x,v) \leq \int_{\mathcal{V}} f(t,x,v')\, dv'.$$

Integrating along the trajectories, we find

$$f(t,x,v) \leq f^0(x - tv, v) + \int_0^t \rho(s, x + (s-t)v)\, ds. \tag{2.5}$$

We can bound the right hand side term by its $L^\infty_x$ norm. Integrating with respect to $v$ provides

$$\|\rho(t,\cdot)\|_{L^\infty(\mathbb{R}^2)} \leq 2\pi \|f^0\|_{L^\infty(\Omega)} + 2\pi \int_0^t \|\rho(s,\cdot)\|_{L^\infty(\mathbb{R}^2)}\, ds.$$

We obtain a bound on the $L^\infty$ norm on $\rho$ thanks to Gronwall's inequality and conclude the proof with (2.5).

□

**Proof of Theorem 2.2.** The local-in-time existence is obtained by a fixed point argument. Let $t_0 > 0$, the map $\mathcal{F}$ on $L^1((0,t_0); L^\infty(\Omega))$ is defined for all $f$ by : $\mathcal{F}(f)$ is a weak solution of the problem

$$\begin{cases} \partial_t \mathcal{F} + v \cdot \nabla_x \mathcal{F} = & \displaystyle\int_{v' \in \mathcal{V}} \phi(\nabla_x G * (v'\rho - J)) \mathcal{F}(v')\, dv' - 2\pi \phi(\nabla_x G * (v\rho - J)) \mathcal{F}(v), \\ \mathcal{F}(0,\cdot,\cdot) = f^0, \end{cases}$$

where $\rho = \int_{\mathcal{V}} f(t,x,v)\, dv$ and $J = \int_{\mathcal{V}} v f(t,x,v)\, dv$. We will show that this map defines a contraction on $L^1((0,\tau), L^\infty(\Omega))$ for $\tau$ small enough. Let $f_1$ and $f_2$ be given in $L^1((0,t_0), L^\infty(\Omega))$ and denoting $\mathcal{F}_{12} = \mathcal{F}(f_1) - \mathcal{F}(f_2)$ we have

$$\begin{aligned} \partial_t \mathcal{F}_{12} + v \cdot \nabla_x \mathcal{F}_{12} = & \int_{\mathcal{V}} \phi(\nabla_x \cdot G * (v\rho_1 - J_1)) \mathcal{F}_{12}(v')\, dv' - 2\pi \phi(\nabla_x \cdot G * (v\rho_1 - J_1)) \mathcal{F}_{12} \\ & -2\pi \mathcal{F}(f_2)(\phi(\nabla_x \cdot G * (v\rho_1 - J_1)) - \phi(\nabla_x \cdot G * (v\rho_2 - J_2)) \\ & + \int_{\mathcal{V}} \mathcal{F}(f_2)(v')(\phi(\nabla_x \cdot G * (v'\rho_1 - J_1)) - \phi(\nabla_x \cdot G * (v'\rho_2 - J_2))\, dv', \end{aligned}$$

with the notations $\rho_i = \int_{\mathcal{V}} f_i(t,x,v)\,dv$ and $J_i = \int_{\mathcal{V}} v f_i(t,x,v)\,dv$. We can rewrite this identity in the following way

$$\partial_t \mathcal{F}_{12} + v\cdot\nabla_x \mathcal{F}_{12} + 2\pi\phi(\nabla_x\cdot G * (v\rho_1 - J_1))\mathcal{F}_{12} = \mathcal{G}, \tag{2.6}$$

where

$$\mathcal{G}(t,x,v) = \int_{\mathcal{V}} \phi(\nabla_x\cdot G*(v'\rho_1 - J_1))\mathcal{F}_{12}(v')\,dv' - 2\pi\mathcal{F}(f_2)(\phi(\nabla_x\cdot G*(v\rho_1-J_1))- \\ \phi(\nabla_x\cdot G*(v\rho_2-J_2)) + \int_{\mathcal{V}} \mathcal{F}(f_2)(v')(\phi(\nabla_x\cdot G*(v'\rho_1-J_1)) - \phi(\nabla_x\cdot G*(v'\rho_2-J_2))\,dv'. \tag{2.7}$$

Using the characteristics of the system, we can rewrite equation (2.6) as

$$\frac{d}{ds}\left(e^{2\pi\phi(\nabla_x\cdot G*(v\rho_1-J_1))(\tau,x+v(\tau-t))}\mathcal{F}_{12}(s,x+v(s-t),v)\right) = \\ e^{2\pi\phi(\nabla_x\cdot G*(v\rho_1-J_1))(\tau,x+v(\tau-t))}\mathcal{G}(s,x+v(s-t),v).$$

At the initial time, $\mathcal{F}_{12}(0,\cdot,\cdot)=0$. Integrating the latter equality between 0 and $t$, we have

$$\mathcal{F}_{12}(t,x,v) = \int_0^t \exp\left(2\pi\int_t^s \phi(\nabla_x\cdot G*(v\rho_1-J_1))(\tau,x+v(\tau-t))\,d\tau\right)\mathcal{G}(s,x+v(s-t),v)\,ds.$$

Since $\phi$ (1.4) is bounded from below by $1/4$ we deduce that for all $0<t<t_0$,

$$|\mathcal{F}_{12}(t,x,v)| \le \int_0^t |\mathcal{G}(t-s,x-vs,v)|\,ds. \tag{2.8}$$

Moreover, from (2.7) and the assumptions on $\phi$ (1.4), we deduce

$$|\mathcal{G}| \le \int_{\mathcal{V}} |\mathcal{F}_{12}(v')|\,dv' + \|\phi'\|_\infty\left(2\pi\mathcal{F}(f_2) + \int_{\mathcal{V}}\mathcal{F}(f_2)(v')\,dv'\right)\times \\ \times\left(|\nabla_x G*(J_1-J_2)| + V|\nabla_x G*(\rho_1-\rho_2)|\right),$$

where $V = \max_{v\in\mathcal{V}}\|v\|$. Noticing that $|J_1-J_2|\le V|\rho_1-\rho_2|$, we have moreover

$$\||\nabla_x G*(J_1-J_2)(t,\cdot)| + V|\nabla_x G*(\rho_1-\rho_2)(t,\cdot)|\|_{L^\infty(\mathbb{R}^2)} \le V\|\nabla_x G\|_{L^1(\mathbb{R}^2)}\|(\rho_1-\rho_2)(t,\cdot)\|_{L^\infty(\mathbb{R}^2)}.$$

Finally, from (2.8) we deduce the bound

$$\|\mathcal{F}_{12}(t,\cdot,\cdot)\|_{L^\infty(\Omega)} \le C_1\int_0^t \|\mathcal{F}_{12}(t-s,\cdot,\cdot)\|_{L^\infty(\Omega)}\,ds + \\ C_2\int_0^t \|\mathcal{F}(f_2)(t-s,\cdot,\cdot)\|_{L^\infty(\Omega)}\|\nabla_x G\|_{L^1(\mathbb{R}^2)}\|(\rho_1-\rho_2)(t-s,\cdot)\|_{L^\infty(\mathbb{R}^2)}\,ds.$$

Therefore, using a Gronwall Lemma, we conclude that for $\tau>0$ small enough, $\mathcal{F}$ defines a contraction on $L^1((0,\tau),L^\infty(\Omega))$. It allows to construct a unique solution as the fixed point of the map $\mathcal{F}$ on the interval $(0,\tau)$. Using the a priori estimates established in Lemma 2.3, we can extend this solution on $(0,t_0)$ for all $t_0>0$ and we have a bound on this solution in $L^\infty(0,t_0;L^1\cap L^\infty(\Omega))$.

For the proof of the second point of Theorem 2.2, let us assume that $f^0 \in W^{2,\infty}(\Omega)$ and that $t_0 > 0$ is fixed. By differentiating with respect to $x_1$ the kinetic equation (2.3) satisfied by $f$, we obtain

$$\begin{aligned}\partial_t \partial_{x_1} f + v \cdot \nabla_x \partial_{x_1} f + 2\pi\phi(\nabla_x \cdot G * (v\rho - J))\partial_{x_1} f = \textstyle\int_{\mathcal{V}} \phi(\nabla_x \cdot G * (v'\rho - J))\partial_{x_1} f(v')\, dv' \\ + \textstyle\int_{\mathcal{V}} \nabla_x G * (v'\partial_{x_1}\rho - \partial_{x_1} J)\phi'(\nabla_x G * (v'\rho - J)) f(v')\, dv' \\ -2\pi\nabla_x G * (v\partial_{x_1}\rho - \partial_{x_1} J)\phi'(\nabla_x G * (v\rho - J)) f(v).\end{aligned}$$

The right hand side is bounded by

$$\int_{\mathcal{V}} |\partial_{x_1} f(v')|\, dv' + 8\pi V \|\phi'\|_{L^\infty} \|f\|_{L^\infty(\Omega)} \|\nabla_x G\|_{L^1(\Omega)} \int_{\mathcal{V}} |\partial_{x_1} f(v')\, dv'|.$$

Integrating along the characteristics and proceeding as above, we obtain that for all $0 \le t \le t_0$,

$$|\partial_{x_1} f(t,x,v)| \le C_1 |\partial_{x_1} f^0(x - tv, v)| + C_2 \int_0^t \int_{\mathcal{V}} |\partial_{x_1} f(t-s, x - sv, v)|\, ds,$$

where $C_1$ and $C_2$ stand for nonnegative constants depending only on $t_0$ and on the data. By the same token as in proof of Lemma 2.3 using Gronwall's inequality, we obtain a bound on $\partial_{x_1} f$ in $L^\infty((0,t_0); L^\infty(\Omega))$. Differentiating (2.3) with respect to $x_2$ and $v$, we deduce by the same token that for all $t \in (0,t_0)$, we have $f(t,\cdot,\cdot) \in W^{1,\infty}(\Omega)$. With a similar argument we deduce after straightforward calculations that $f$ is bounded in $L^\infty((0,t_0); W^{2,2}(\Omega))$. Moreover from (2.3) we have an expression of $\partial_t f$ with respect to $f$, $\rho$, $J$, $\nabla_x G$ and $\nabla_x f$ allowing to obtain a bound on $\partial_t f$ in $L^\infty((0,t_0); L^\infty(\Omega))$. □

**Remark 2.4** *For the sake of simplicity, this existence result has been established in the domain $\omega = \mathbb{R}^2$. However, this existence and uniqueness result is still available in a bounded domain $\omega \subset \mathbb{R}^2$ provided that the boundary conditions allows to use the elliptic regularity for the elliptic equation satisfied by $S$. For numerical analysis, we will constraint the domain $\omega$ to be bounded and make use of this existence result in this framework.*

# 3 Numerical approach

In this section, we present the numerical approach for solving (1.5). The computational domain is defined by $(x,v) \in \Omega = \omega \times \mathbb{S}_V$ where $\omega$ is a rectangular domain of $\mathbb{R}^2$, $\omega = [0, L_x] \times [0, \ell_y]$, and $\mathbb{S}_V$ is the sphere $\mathbb{S}_V = \{v \in \mathbb{R}^2, \text{ such that } \|v\|_2 = V\}$, for a given constant velocity $V > 0$. We reduce this 4-dimensional problem to a 3-dimensional problem by considering the cylindrical coordinate $\theta$.

At the boundary of the domain, we assume to have specular reflection at the boundaries $y = 0$, $y = \ell_y$, $x = 0$ and $x = L_x$ for the distribution function; for the chemoattractant

concentration $S$ we set Neumann conditions on the entire boundary :

$$\begin{aligned}
&f(x,0,\theta) = f(x,0,2\pi-\theta), && \text{for } \theta\in[0,\pi], \quad x\in[0,L_x],\\
&f(x,\ell_y,\theta) = f(x,\ell_y,2\pi-\theta), && \text{for } \theta\in[\pi,2\pi], \quad x\in[0,L_x],\\
&f(0,y,\theta) = f(0,y,\pi-\theta), && \text{for } \theta\in[0,\pi/2]\cup[3\pi/2,2\pi], \quad y\in[0,\ell_y],\\
&f(L_x,y,\theta) = f(L_x,y,\pi-\theta), && \text{for } \theta\in[\pi/2,3\pi/2], \quad y\in[0,\ell_y],\\
&\partial_x S(0,y) = \partial_x S(L_x,y) = 0, && \text{for } y\in[0,\ell_y],\\
&\partial_y S(x,0) = \partial_y S(x,\ell_y) = 0, && \text{for } x\in[0,L_x].
\end{aligned} \tag{3.1}$$

Obviously, in the $\theta$ direction f is $2\pi$-periodic.

We introduce the nodes $(x_i = i\,h_x)_{i=0,\cdots,N_x-1}$, $(y_j = j\,h_y)_{j=0,\cdots,N_y-1}$ and $(\theta_k = k\,h_\theta)_{\theta=0,\cdots,N_\theta-1}$ where $h_x = L_x/(N_x-1)$, $h_y = \ell_y/(N_y-1)$ and $h_\theta = 2\pi/N_\theta$. We denote $\mathbf{x_i} = (x_{i_1}, y_{i_2})$ with $i = i_1 + i_2\,N_x$ and we mesh the domain $\omega$ with rectangular triangles using the nodes $\mathbf{x_i}$. Therefore the triangulation is regular and all finite elements are affine equivalent to a single reference element. We denote the time step $\Delta t$ and set $t^n = n\,\Delta t$ for $n = 0,\ldots,N_t$.

## 3.1 Semi-Lagrangian methods

In this section we describe the semi-Lagrangian method used for the numerical resolution in $\omega\subset\mathbb{R}^2$ of the kinetic equation :

$$\partial_t f + v\cdot\nabla_x f = \int_{\mathbb{S}_V} \phi(\partial_t S + v'\cdot\nabla_x S) f(v')\,dv' - 2\pi\phi(\partial_t S + v\cdot\nabla_x S) f(v), \tag{3.2}$$

completed with the initial datum (1.2). We assume in this section that the chemoattractant concentration is known and we will therefore consider the turning kernel as a function of $t$, $x$ and $v$ : $T(t,x,v) = \phi(\partial_t S(t,x) + v\cdot\nabla_x S(t,x))$. Its numerical approximation will be denoted $T_h$.

Semi-Lagrangian methods consist in calculating the distribution function at time $t^{n+1} = t^n + \Delta t$ thanks to the one which has been obtained at the time $t^n$ by using the conservation relation along the characteristics curves. We first define the characteristics $(X,\Theta)$ of the system for all $0\le s\le t$ by :

$$\left\{\begin{array}{ll}
\dfrac{d}{ds}X(s;\mathbf{x},\theta,t) = \mathbf{v_\Theta}, & \text{with } \mathbf{v_\Theta} = (V\cos\Theta, V\sin\Theta)\ ; \qquad X(t;\mathbf{x},\theta,t) = \mathbf{x},\\
\dfrac{d}{ds}\Theta(s;\mathbf{x},\theta,t) = 0\ ; & \qquad \Theta(t;\mathbf{x},\theta,t) = \theta,
\end{array}\right. \tag{3.3}$$

if $X(s;\mathbf{x},\theta,t)\in(0,L_x)\times(0,\ell_y)$. Therefore the velocity remains constant, except when the trajectory meets a boundary of the domain : if there exists a time $s>0$ such that $X(s;\mathbf{x},\theta,t)\in(0,L_x)\times\{0,\ell_y\}$ then the angle $\Theta(s;\mathbf{x},\theta,t)$ is changed into $2\pi-\Theta(s;\mathbf{x},\theta,t)$; if there exists a time $s>0$ such that $X(s;\mathbf{x},\theta,t)\in\{0,L_x\}\times(0,\ell_y)$ then $\Theta(s;\mathbf{x},\theta,t)$ is substituted by $\pi-\Theta(s;\mathbf{x},\theta,t)$. More precisely, we have

$$X(s;\mathbf{x},\theta,t) = \mathbf{x} + \mathbf{v}_\theta(s-t), \qquad \text{with } \mathbf{v}_\theta = (V\cos\theta, V\sin\theta), \qquad \Theta(s;\mathbf{x},\theta,t) = \theta,$$

for all $s\in\mathbb{R}^+$ for which the trajectory does not cross the boundaries. By reflection, if the trajectory reaches one of the boundaries $y=0$ or $y=\ell_y$ only once at time $t_0$, then for

$t < t_0 < s$,

$$X(s;\mathbf{x},\theta,t) = \mathbf{x} + \mathbf{v}_\theta(t_0 - t) + \mathbf{v}_{\mathbf{2\pi-\theta}}(s - t_0) \qquad \text{and} \qquad \Theta(s;\mathbf{x},\theta,t) = 2\pi - \theta.$$

If the trajectory crosses the boundary $x = 0$ or $x = L_x$ at time $t_1$, then for $t < t_1 < s$, we have

$$X(s;\mathbf{x},\theta,t) = \mathbf{x} + \mathbf{v}_\theta(t_1 - t) + \mathbf{v}_{\pi-\theta}(s - t_1) \qquad \text{and} \qquad \Theta(s;\mathbf{x},\theta,t) = \pi - \theta.$$

Obviously, if the trajectory meets several times the boundaries, we make others reflections. Using the characteristics, we can rewrite the kinetic equation (3.2) in the following way :

$$\begin{aligned}\frac{d}{ds} f(s, X(s;\mathbf{x},\theta,t), \Theta(s;\mathbf{x},\theta,t)) = \int_0^{2\pi} (T(s, X(s;\mathbf{x},\theta,t),\theta') f(s, X(s;\mathbf{x},\theta,t),\theta')\, d\theta' \\ -2\pi\, T(s, X(s;\mathbf{x},\theta,t), \Theta(s;\mathbf{x},\theta,t))\, f(s, X(s;\mathbf{x},\theta,t), \Theta(s;\mathbf{x},\theta,t))).\end{aligned} \tag{3.4}$$

The semi-Lagrangian method relies on a discrete approximation of relation (3.4). We assume to know the distribution function at time $t^n$ . We use an explicit in time Euler scheme to compute this quantity at time $t^{n+1} = t^n + \Delta t$ on each point $(\mathbf{x_i}, \theta_j)$ of the grid. It leads to the following system :

$$\begin{aligned} f_h(t^{n+1}, \mathbf{x_i}, \theta_j) = f_h(t^{n+1}, X(t^n;\mathbf{x_i},\theta_j,t^{n+1}), \Theta(t^n;\mathbf{x_i},\theta_j,t^{n+1})) \\ +\Delta t \int_0^{2\pi} (T_h(t^n, X(t^n;\mathbf{x_i},\theta_j,t^{n+1}),\theta') f_h(X(t^n;\mathbf{x_i},\theta_j,t^{n+1}),\theta')\, d\theta' \\ -2\pi\Delta t\, T_h(t^n, X(t^n;\mathbf{x_i},\theta_j,t^{n+1}), \Theta(t^n;\mathbf{x_i},\theta_j,t^{n+1}))\, f_h(X(t^n;\mathbf{x_i},\theta_j,t^{n+1}), \Theta(t^n;\mathbf{x_i},\theta_j,t^{n+1}))), \end{aligned} \tag{3.5}$$

where $f_h$ and $T_h$ stand for approximations of $f$ and $T$. For the sake of clarity, we will use from now on the notations $X^n_{i,j}(s)$ instead of $X(s;\mathbf{x_i},\theta_j,t^n)$ and $\Theta^n_{i,j}(s)$ instead of $\Theta(s;\mathbf{x_i},\theta_j,t^n))$. The discretization relies on two main steps :

1. Find the point $(X(t^n;\mathbf{x_i},\theta_j,t^n+\Delta t), \Theta(t^n;\mathbf{x_i},\theta_j,t^n+\Delta t)) := (X^{n+1}_{i,j}(t^n), \Theta^{n+1}_{i,j}(t^n))$. Starting from $(\mathbf{x_i},\theta_j)$, it suffices to follow backward the characteristics curves during the time step $\Delta t$. To this end, we have to solve (3.3). Since the resolution of the second equation in (3.3) is clear, this step is simple (in a general framework see e.g. [39, 2, 15])

   $$X^{n+1}_{i,j}(t^n) = \mathbf{x_i} - \Delta t\, \mathbf{v}_{\mathbf{\Theta^{n+1}_{i,j}}}, \qquad \Theta^{n+1}_{i,j}(t^n) = \theta_j.$$

   Obviously, if the trajectory reaches a boundary of the domain, then we use specular reflection : $X^{n+1}_{i,j}(t^n)$ is replaced by its symmetric with respect to this boundary and $\Theta^{n+1}_{i,j}(t^n)$ by $2\pi - \Theta^{n+1}_{i,j}(t^n)$ at the vertical boundary $y = 0$ or $y = \ell_y$, or by $\pi - \Theta^{n+1}_{i,j}(t^n)$ at the boundary $x = 0$ or $x = L_x$.

   Therefore the computation of the foot of the characteristics is exact.

2. Since the functions $f$ and $T$ at time $t^n$ are only known on the nodes of the mesh, we interpolate these functions at the points $(X^{n+1}_{i,j}(t^n), \Theta^{n+1}_{i,j}(t^n))$. Actually, since we have $\Theta^{n+1}_{i,j}(t^n) = \theta_j$ or $\pi - \theta_j$ or $2\pi - \theta_j$, by taking $N_\theta$ odd we only have a 2D interpolation method to implement. In fact, we have that $2\pi - \theta_j = \theta_{N_\theta - j}$ and $\pi - \theta_j = \theta_{N_\theta/2 - j}$ if $\theta_j \in (0, \pi)$. Several interpolation methods can be used. To avoid Runge phenomena, we

can use a linear interpolation : we define the linear interpolation operator $\Pi$ onto the space of Lagrangian polynomials of degree lesser than or equal to 1 by :

$$\Pi f(x,y) = \sum_{i=0}^{N_x N_y - 1} f(\mathbf{x_i}) l_i(x,y), \quad \text{with } l_i \in \mathbb{P}^1(\omega) \quad \text{such that} \quad l_i(\mathbf{x_j}) = \delta_{ij}, \tag{3.6}$$

where $\mathbb{P}^1(\omega)$ is the set of piecewise polynomials whose restriction on each triangle of the mesh holds in polynomials function of degree lesser than or equal to 1. The interpolation error estimations in Sobolev spaces give that for all $f \in W^{2,2}(\omega)$ (see [13] Theorem 16.2 p. 128)

$$\|f - \Pi f\|_{L^2(\omega)} \leq C \max\{h_x^2, h_y^2\} \|f\|_{W^{2,2}(\omega)}. \tag{3.7}$$

Moreover, this linear interpolation method preserves the $L^\infty$ bound :

$$\|\Pi f\|_{L^\infty(\omega)} \leq \|f\|_{L^\infty(\omega)}. \tag{3.8}$$

For more precision on solutions, a Hermite spline interpolation method which is a well established high order interpolation method can be used. We refer to [39, 15] for more details about this interpolation step. However, spurious oscillations (e.g. Runge phenomena) can appear with high order interpolation methods.

Finally, using a discretization of the integral in (3.5), the approximation of the distribution function at time $t^{n+1}$ is obtained by

$$\begin{aligned} f_h(t^{n+1}, \mathbf{x_i}, \theta_j) = \; & \Pi f_h(t^n, X_{i,j}^{n+1}(t^n), \Theta_{i,j}^{n+1}(t^n)) - 2\pi\Delta t\, \Pi(T_h f_h)(t^n, X_{i,j}^{n+1}(t^n), \Theta_{i,j}^{n+1}(t^n)) + \\ & + \Delta t \sum_{k=0}^{N_\theta - 1} h_\theta\, \Pi(T_h f_h)(t^n, X_{i,j}^{n+1}(t^n), \theta_k). \end{aligned} \tag{3.9}$$

## 3.2 Numerical resolution of the coupled system

We recall the following notations : $X_{i,j}^{n+1}(t^n)$ instead of $X(t^n; \mathbf{x_i}, \theta_j, t^{n+1})$, $\Theta_{i,j}^{n+1}(t^n)$ instead of $\Theta(t^n; \mathbf{x_i}, \theta_j, t^{n+1}))$ and $\Pi$ is the interpolation operator. The numerical resolution of the coupled problem (1.5) is then tackled in the following way. We assume that the approximation of the distribution function $f_h$ and of the chemoattractant concentration $S_h$ are known at time $t^n$ at each nodes of the mesh. We describe the process to compute $f_h$ and $S_h$ at time $t^{n+1}$. As described previously, the distribution function at time $t^{n+1}$ is approximated thanks to the relation :

$$\begin{aligned} f_h(t^{n+1}, \mathbf{x_i}, \theta_j) = \; & \Pi f_h(t^n, X_{i,j}^{n+1}(t^n), \Theta_{i,j}^{n+1}(t^n)) - 2\pi\Delta t\, \Pi(T_h f_h)(t^n, X_{i,j}^{n+1}(t^n), \Theta_{i,j}^{n+1}(t^n)) + \\ & + \Delta t \sum_{k=0}^{N_\theta - 1} h_\theta\, \Pi(T_h f_h)(t^n, X_{i,j}^{n+1}(t^n), \theta_k), \end{aligned} \tag{3.10}$$

where the turning kernel $T_h$ is computed by a discretization of (1.3). As we have seen for the proof of Theorem 2.2, estimates on $T$ rely on the conservation equation for $\rho$ (2.1) which allows

to get an estimation of the term involving temporal derivative in the definition of $T$. In fact, the quantity $\partial_t S$ satisfies

$$-\Delta \partial_t S + \partial_t S = -\nabla \cdot J, \tag{3.11}$$

completed with Neumann boundary conditions deduced from (3.1). We define the approximation of the current by

$$J_h(t^n, \mathbf{x_i}) = \sum_{k=0}^{N_\theta - 1} h_\theta \mathbf{v}_{\theta_\mathbf{k}} f_h(t^n, \mathbf{x_i}, \theta_k). \tag{3.12}$$

Then the approximation of $\partial_t S$, denoted $S_{th}$, is computed by solving (3.11) with $J_h$ using conforming $\mathbb{P}^1$ finite elements :

$$\forall\, V_h \in X_h, \quad \int_\omega (\nabla S_{th} \cdot \nabla V_h + S_{th} V_h)\, dx = \int_\omega J_h \cdot \nabla V_h\, dx, \tag{3.13}$$

where $X_h$ is the set of function of $C^0(\overline{\omega})$ whose restriction to each triangle on the mesh holds in $\mathbb{P}^1$. We define the approximation $T_h$ of the turning kernel by

$$T_h(t^n, \mathbf{x_i}, \theta_j) = \phi\left( S_{th}(t, \mathbf{x}) + \frac{1}{\Delta t}(S_h(t^n, \mathbf{x_i}) - \Pi S_h(t^n, X^n_{i,j}(t^{n-1}))\right). \tag{3.14}$$

Once $f_h$ is known at time $t^{n+1}$, the chemoattractant concentration is updated by solving the following elliptic equation with conforming $\mathbb{P}^1$ finite elements :

$$-\Delta S_h(t^{n+1}, \mathbf{x_i}) + S_h(t^{n+1}, \mathbf{x_i}) = \rho_h(t^{n+1}, \mathbf{x_i}) := \sum_{k=0}^{N_\theta - 1} f_h(t^{n+1}, \mathbf{x_i}, \theta_k)\, h_\theta. \tag{3.15}$$

This system is completed with boundary conditions (3.1).

From basic error estimates on elliptic problem, we have (see [13] Theorem 18.1 p. 138) :

**Proposition 3.1** *Let $u$ be a solution of the variational problem $a(u, v) = l(v)$ where $a$ is bilinear continuous symmetric coercive on $H^1(\omega)$ and $l$ is linear continuous on $H^1(\omega)$. Then, if $u_h$ is the discrete approximation computed by conforming $\mathbb{P}^1$ finite elements, there exists a nonnegative constant $C$ such that*

$$\|u - u_h\|_{H^1(\omega)} \leq C \max\{h_x, h_y\} \|u\|_{H^2(\omega)}.$$

## 3.3 Convergence analysis

We are interested in this section in the convergence of the scheme (3.10)–(3.15) towards solutions of model (1.5). Convergence analysis of semi-Lagrangian method in the framework of Vlasov-Poisson system have been obtained in [3]; those results are presented in $L^\infty$. Due to the lack of regularity in our case caused by the presence of the turning operator, we present in the following theorem a convergence result in $L^2$. The main result of this section is presented in Theorem 3.4 below under the following additional assumption allowing to simplify all integrals in the computation.

**Assumption 3.2** *For the sake of simplicity of the proof and of the notations, we assume that all particles are initially confined in the center of the device and that the time $t_0$ is small enough to avoid particles to meet the boundary of the domain. Thus all trajectories are straight lines and*

$$X(s;\mathbf{x},\theta,t) = \mathbf{x} + \mathbf{v}_\theta(s-t); \quad \Theta(s;\mathbf{x},\theta,t) = \theta, \quad \text{for } 0 \le s \le t.$$

*Moreover, since $f_h$ vanishes near the boundary of the domain $\omega$, we have*

$$\int_\omega f_h(t, X(s;\mathbf{x},\theta,t),\theta)\,dx = \int_\omega f_h(t,\mathbf{x},\theta)\,dx,$$

*for $0 \le s \le t$ small enough.*

From now on, we fix $t_0 > 0$ small enough and assume $f^0 \in W^{2,2} \cap W^{1,\infty}(\Omega)$ is chosen such that Assumption 3.2 holds. Therefore, in this convergence analysis cells do not 'see' the boundary. The scheme (3.10)–(3.15) allows to define the approximated function $f_h$ only on the nodes on the mesh. We extend this definition on all $(\mathbf{x},\theta) \in \omega \times [0,2\pi]$ thanks to the linear interpolation operator $\Pi$ (3.6). We first establish the positivity and a priori estimates on the discrete approximation $f_h$.

**Lemma 3.3** *Let $t_0 > 0$ and assume that $f^0 \in W^{2,2} \cap W^{1,\infty}(\omega \times [0,2\pi])$ is a nonnegative function such that Assumption 3.2 holds. If $\Delta t \le 1/(2\pi)$, then the scheme defined by* (3.10)–(3.15) *gives a nonnegative approximation $f_h$ of the distribution function. Moreover $f_h$ satisfies the following estimate*

$$\forall\, t \in (0,t_0), \quad \|\Pi f_h(t,\cdot,\cdot)\|_{L^\infty(\omega\times[0,2\pi])} \le e^{2\pi t_0}\|f^0\|_{L^\infty(\omega\times[0,2\pi])}, \quad \|\Pi f_h(t,\cdot,\cdot)\|_{H^1(\omega\times[0,2\pi])} \le C_0,$$

*where $C_0$ is a nonnegative constant depending on $t_0$ and $\|f^0\|_{H^1(\omega\times[0,2\pi])}$.*

**Proof.** From the definition of (3.6) and the assumptions on $\phi$ (1.4) we have that for all nonnegative function $f$

$$\frac{1}{4}\Pi f \le \Pi(Tf) \le \Pi f.$$

Therefore assuming $f(t^n,\cdot,\cdot)$ nonnegative, we deduce from (3.10) that

$$f_h(t^{n+1},\mathbf{x_i},\theta_j) \ge (1-2\pi\Delta t)\,\Pi f_h(t^n,\mathbf{x_i}-\mathbf{v}_{\theta_j}\Delta t,\theta_j) \ge 0.$$

Moreover, from (3.10) and (3.8) we have

$$\|\Pi f_h(t^{n+1},\cdot,\cdot)\|_{L^\infty(\omega\times[0,2\pi])} \le (1+2\pi\Delta t)\,\|\Pi f_h(t^n,\cdot,\cdot)\|_{L^\infty(\omega\times[0,2\pi])}.$$

Applying a discrete Gronwall inequality allows to conclude the proof of the $L^\infty$ bound. Differentiating (3.10) with respect to $x_1$ gives

$$\begin{aligned}\partial_{x_1} f_h(t^{n+1},\mathbf{x_i},\theta_j) &= \partial_{x_1}\Pi f_h(t^n,\mathbf{x_i}-\mathbf{v}_{\theta_j}\Delta t,\theta_j)\\ -2\pi\Delta t\,\partial_{x_1}\Pi(T_h f_h)(t^n,\mathbf{x_i}-\mathbf{v}_{\theta_j}\Delta t,\theta_j) &+ \Delta t\textstyle\sum_{k=0}^{N_\theta-1} h_\theta\,\partial_{x_1}\Pi(T_h f_h)(t^n,\mathbf{x_i}-\mathbf{v}_{\theta_j}\Delta t,\theta_k).\end{aligned} \tag{3.16}$$

By linearity of the interpolation operator, we have that

$$\partial_{x_1}\Pi(T_h f_h) = \Pi(\partial_{x_1}[(\Pi T_h)(\Pi f_h)]) = \Pi(\partial_{x_1}(\Pi T_h)\Pi f_h + (\Pi T_h)\partial_{x_1}(\Pi f_h)).$$

From the definition of $T_h$ (3.14), we deduce that

$$\|\partial_{x_1}(\Pi T_h)(t^n)\|_{L^2(\omega)} \leq \|\partial_{x_1} S_{th}(t^n)\|_{L^2(\omega)} + \frac{1}{\Delta t}\|\partial_{x_1} S_h(t^n,\cdot) - \partial_{x_1}\Pi S_h(t^n, X(t^{n-1};\cdot,\theta,t^n))\|_{L^2(\omega)}.$$

From the elliptic regularity on the equation (3.13) and the bound of $f_h$ in $L^\infty(\omega\times[0,2\pi])$, we have that $S_{th}$ is bounded in $H^1(\omega)$. The elliptic regularity on (3.15) gives

$$\|S_h(t^n,\cdot) - \Pi S_h(t^n, X(t^{n-1};\cdot,\theta,t^{n-1}))\|_{H^1(\omega)} \leq \|\rho_h(t^n,\cdot) - \Pi\rho_h(t^n, X(t^{n-1};\cdot,\theta,t^n))\|_{L^2(\omega)}.$$

Using a Taylor expansion gives

$$\rho_h(t^n,\mathbf{x}) - \Pi\rho_h(t^n,\mathbf{x}-\mathbf{v}_\theta\Delta t) = \int_{-\Delta t}^{0} \mathbf{v}_\theta\cdot\nabla\Pi\rho_h(t,\mathbf{x}+\mathbf{v}_\theta s)\,ds.$$

From Assumption 3.2 we deduce that

$$\|\rho_h(t^n,\mathbf{x}) - \Pi\rho_h(t^n,\mathbf{x}-\mathbf{v}_\theta\Delta t)\|_{L^2(\omega)} \leq \Delta t V\|\nabla(\Pi\rho_h)(t^n,\cdot)\|_{L^2(\omega)}.$$

Thus,

$$\|\partial_{x_1}(\Pi T_h)\|_{L^2(\omega\times[0,2\pi])} \leq C(1+\|\nabla(\Pi\rho_h)\|_{L^2(\omega\times[0,2\pi])}).$$

Doing the same with $x_2$, (3.16) leads to the following estimate

$$\|\nabla\Pi f_h(t^{n+1})\|_{L^2(\omega\times[0,2\pi])} = \|\nabla\Pi f_h(t^n)\|_{L^2(\omega\times[0,2\pi])} + C\Delta t(1+\|\nabla\Pi f_h(t^n)\|_{L^2(\omega\times[0,2\pi])}).$$

A Gronwall inequality allows to conclude the proof. □

**Theorem 3.4** *Let $t_0 > 0$ and assume that $f^0 \in W^{2,2}\cap W^{1,\infty}(\omega\times[0,2\pi])$ is a nonnegative function such that Assumption 3.2 holds. Let $f$ be the global weak solution of (1.5) on $(0,t_0)$ and $f_h$ be its approximation computed at the nodes of the mesh thanks to the algorithm (3.10)–(3.15) where $\Pi$ is defined in (3.6). Then there exists a nonnegative constant $C$ depending on $t_0$, $f^0$ and the data such that*

$$\|f - \Pi f_h\|_{L^\infty(0,t_0;L^2(\omega\times[0,2\pi]))} \leq C(\Delta t + h^2 + \frac{h}{\Delta t} + h),$$

*where $h = \max\{h_x, h_y, h_\theta\}$.*

**Proof.** From Theorem 2.2 we have $f(t,\cdot,\cdot)\in W^{1,\infty}\cap W^{2,2}(\omega\times[0,2\pi])$ We define the global error at time $t^{n+1}$ by

$$\epsilon^{n+1} = \|f(t^{n+1},\mathbf{x},\theta) - \Pi f_h(t^{n+1},\mathbf{x},\theta)\|_{L^2(\omega\times[0,2\pi])}. \tag{3.17}$$

A first remark is that since characteristics are straight lines the numerical computation of the characteristics $(X,\Theta)$ is exact. From (1.5), we deduce that for $0\leq s\leq t$

$$\begin{aligned}\frac{d}{ds}f(s,\mathbf{x}-\mathbf{v}_\theta(t-s),\theta) = &\int_0^{2\pi} T(s,\mathbf{x}-\mathbf{v}_\theta(t-s),\theta')f(s,\mathbf{x}-\mathbf{v}_\theta(t-s),\theta')\,d\theta'\\ &-2\pi\,T(s,\mathbf{x}-\mathbf{v}_\theta(t-s),\Theta^n(s))f(s,\mathbf{x}-\mathbf{v}_\theta(t-s),\theta),\end{aligned}$$

where

$$T(t,\mathbf{x},\theta) = \phi(\partial_t S + \mathbf{v}_\theta \cdot \nabla_{\mathbf{x}} S),$$

and $S$ being the solution of the elliptic problem

$$-\Delta S + S = \int_0^{2\pi} f(t,\mathbf{x},\theta)\, d\theta.$$

We deduce from the regularity of the function $f$ proved in Theorem 2.2 that the function $s \mapsto f(s,\mathbf{x}-\mathbf{v}_\theta(t-s),\theta)$ is bounded in $W^{2,2}(0,t_0)$. Hence a Taylor expansion gives, under Assumption 3.2 :

$$\begin{aligned} f(t^{n+1},\mathbf{x},\theta) = f(t^n,\mathbf{x}-\mathbf{v}_\theta\Delta t,\theta) + \Delta t \int_0^{2\pi} T(t^n,\mathbf{x}-\mathbf{v}_\theta\Delta t,\theta') f(t^n,\mathbf{x}-\mathbf{v}_\theta\Delta t,\theta')\, d\theta' \\ -2\pi\Delta t\, T(t^n,\mathbf{x}-\mathbf{v}_\theta\Delta t,\theta) f(t^n,\mathbf{x}-\mathbf{v}_\theta\Delta t,\theta) + O_{L^2}(\Delta t^2), \end{aligned}$$

where $O_{L^2}(\Delta t)$ means that there exists $C>0$ such that $\|O_{L^2}(\Delta t^2)\|_{L^2} \le C\Delta t^2$. Therefore, using the definition (3.10), we rewrite the difference $f(t^{n+1},\mathbf{x},\theta) - \Pi f_h(t^{n+1},\mathbf{x},\theta)$ as

$$\begin{aligned} f(t^{n+1},\mathbf{x},\theta) - \Pi f_h(t^{n+1},\mathbf{x},\theta) = f(t^n,\mathbf{x}-\mathbf{v}_\theta\Delta t,\theta) - \Pi f_h(t^n,\mathbf{x}-\mathbf{v}_\theta\Delta t,\theta) \\ +\Delta t \left( \int_0^{2\pi} (Tf)(t^n,\mathbf{x}-\mathbf{v}_\theta\Delta t,\theta')\, d\theta' - \sum_{k=0}^{N_\theta-1} h_\theta\, \Pi(T_h f_h)(t^n,\mathbf{x}-\mathbf{v}_\theta\Delta t,\theta_k) \right) \\ -2\pi\Delta t\, ((Tf)(t^n,\mathbf{x}-\mathbf{v}_\theta\Delta t,\theta) - \Pi(T_h f_h)(t^n,\mathbf{x}-\mathbf{v}_\theta\Delta t,\theta)) + O_{L^2}(\Delta t^2). \end{aligned}$$

To evaluate the global error $\epsilon^{n+1}$, we decompose $f(t^{n+1},\mathbf{x},\theta) - f_h(t^{n+1},\mathbf{x},\theta)$ as

$$\begin{aligned} f(t^{n+1},\mathbf{x},\theta) - \Pi f_h(t^{n+1},\mathbf{x},\theta) = \quad & f(t^n,\mathbf{x}-\mathbf{v}_\theta\Delta t,\theta) - \Pi f_h(t^n,\mathbf{x}-\mathbf{v}_\theta\Delta t,\theta) \\ & +\Delta t((1-\Pi)I_1 + I_2 + I_3) + O_{L^2}(\Delta t^2), \end{aligned} \tag{3.18}$$

where

$$I_1 = \sum_{k=0}^{N_\theta-1} h_\theta (Tf)(t^n,\mathbf{x}-\mathbf{v}_\theta\Delta t,\theta_k) - 2\pi(Tf)(t^n,\mathbf{x}-\mathbf{v}_\theta\Delta t,\theta), \tag{3.19}$$

$$I_2 = \sum_{k=0}^{N_\theta-1} h_\theta (Tf - T_h f_h)(t^n,\mathbf{x}-\mathbf{v}_\theta\Delta t,\theta_k) - 2\pi(Tf - T_h f_h)(t^n,\mathbf{x}-\mathbf{v}_\theta\Delta t,\theta), \tag{3.20}$$

$$I_3 = \int_0^{2\pi} (Tf)(t^n,\mathbf{x}-\mathbf{v}_\theta\Delta t,\theta')\, d\theta' - \sum_{k=0}^{N_\theta-1} h_\theta (Tf)(t^n,\mathbf{x}-\mathbf{v}_\theta\Delta t,\theta_k). \tag{3.21}$$

Taking the $L^2$ norm of (3.18) implies with Assumption 3.2

$$\epsilon^{n+1} \le \epsilon^n + \Delta t(\|(1-\Pi)I_1\|_{L^2(\omega\times[0,2\pi])} + \|I_2\|_{L^2(\omega\times[0,2\pi])} + \|I_3\|_{L^2(\omega\times[0,2\pi])}) + C\Delta t^2. \tag{3.22}$$

We will estimate each term separately thanks to the following Lemmata.

**Lemma 3.5** *Let $(f,S)$ being solution of (1.5) for $f^0 \in W^{1,\infty} \cap W^{2,2}(\omega\times[0,2\pi])$. If $I_1$ is defined by (3.19), then there exists a nonnegative constant $C$ such that for all $t \in (0,t_0)$,*

$$\|(1-\Pi)I_1\|_{L^2(\omega\times[0,2\pi])} \le C \max\{h_x^2, h_y^2\}.$$

**Proof.** Let $0 \leq t \leq t_0$. From Theorem 2.2, we have that $f(t,\cdot,\cdot) \in W^{1,\infty} \cap W^{2,2}(\omega \times [0,2\pi])$. Therefore, by elliptic regularity, we deduce that $\nabla S(t,\cdot) \in W^{3,2}(\omega)$. Moreover, (3.11) implies

$$-\Delta \partial_t S(t,\cdot) + \partial_t S(t,\cdot) = -\nabla \cdot J(t,\cdot) \in W^{1,2}(\omega).$$

Then the elliptic regularity furnishes $\partial_t S(t,\cdot) \in W^{3,2}(\omega)$ and since with our definition on $\phi$ we get $\phi' \in C_c^\infty(\mathbb{R})$, we deduce that $T(t,\cdot,\cdot) = \phi(\partial_t S + \mathbf{v}_\theta \cdot \nabla S) \in W^{3,2}(\omega \times [0,2\pi])$. Then

$$\partial^2_{x_i x_j}(Tf) = (\partial_{x_i x_j} T) f + \partial_{x_i} T \partial_{x_j} f + \partial_{x_j} T \partial_{x_i} f + T(\partial_{x_i x_j} f) \quad \in L^2(\omega \times [0,2\pi]).$$

Hence $(T\,f)(t,\cdot,\cdot) \in W^{2,2}(\omega \times [0,2\pi])$. Finally, the result of the Lemma is a straightforward consequence of the interpolation error (3.7). □

**Lemma 3.6** *Let $f$ and $T$ being defined previously, there exists a nonnegative constant $C$ such that for all $0 \leq t \leq t_0$ and $\mathbf{x} \in \omega$,*

$$\left\| \int_0^{2\pi} (Tf)(t,\mathbf{x},\theta')\, d\theta' - \sum_{k=0}^{N_\theta - 1} h_\theta (Tf)(t,\mathbf{x},\theta_k) \right\|_{L^2(\omega)} \leq C h_\theta^2.$$

**Proof.** Let $0 \leq t \leq t_0$ and $x \in \omega$. As noticed in the proof of Lemma 3.5 we have that $(T\,f)$ belongs to $W^{2,2}(\omega \times [0,2\pi])$. Hence the result of Lemma 3.6 is a consequence of the well-known error estimate for the trapezoidal rule : if $g \in W^{2,2}(0,2\pi)$, there exists $\theta \in (0,2\pi)$ such that

$$\left| \int_0^{2\pi} g(\theta)\, d\theta - \sum_{k=0}^{N_\theta - 1} h_\theta g(\theta_k) \right| = h_\theta^2 \frac{\pi}{6} \left| \frac{\partial^2 g(\theta)}{\partial \theta^2} \right|. \tag{3.23}$$

□

The two previous Lemmata allow us to estimate the terms involving $I_1$ and $I_3$ in (3.22). For $I_2$, we need first to estimate the error $T - T_h$ with respect to $f - f_h$.

**Lemma 3.7** *Let assume that Assumption 3.2 holds. Let $T$ be defined in* (1.3)–(1.4) *and $T_h$ be its approximation computed with* (3.14). *Then, there exists $C > 0$ such that for $n = 1, \ldots, N_t$, we have*

$$\begin{aligned} \| \sup_{\alpha \in [0,2\pi]} |T(t^n,\cdot,\alpha) - \Pi T_h(t^n,\cdot,\alpha)| \|_{L^2(\omega)} \leq \; & C(\Delta t + \max\{h_x,h_y\} + \frac{\max\{h_x,h_y\}}{\Delta t} + h_\theta^2 + \\ & + \|f(t^n,\cdot,\cdot) - f_h(t^n,\cdot,\cdot)\|_{L^2(\omega \times [0,2\pi])}). \end{aligned}$$

**Proof.** Let $n \in \{1, \ldots, N_t\}$, $\mathbf{x} \in \omega$ and $\alpha \in [0,2\pi]$. We have from (3.14) that

$$\begin{aligned} & |T(t^n,\mathbf{x},\alpha) - \Pi T_h(t^n,\mathbf{x},\alpha)| = |\phi(\partial_t S(t^n,\mathbf{x}) + \mathbf{v}_\alpha \cdot \nabla_x S(t^n,\mathbf{x})) - \Pi T_h(t^n,\mathbf{x},\alpha)| \\ & \leq \|\phi'\|_{L^\infty} (|\partial_t S(t^n,\mathbf{x}) - S_{th}(t^n,\mathbf{x})| + |\mathbf{v}_\alpha \cdot \nabla_x S(t^n,\mathbf{x}) - \frac{1}{\Delta t}(S_h(t^n,\mathbf{x}) - \Pi S_h(t^n,\mathbf{x} - \mathbf{v}_\alpha \Delta t))|), \end{aligned} \tag{3.24}$$

where $S_{th}$ is defined in (3.13). We will estimate separately each term of the sum of the right hand side. Let us introduce $\widetilde{S}_t$ a weak solution of

$$-\Delta \widetilde{S}_t + \widetilde{S}_t = -\nabla \cdot \Pi J_h, \tag{3.25}$$

completed with Neumann boundary conditions, where $J_h$ is defined in (3.12) at the nodes of the mesh and extended on $\omega$ thanks to the linear interpolation operator $\Pi$. From Proposition 3.1, we deduce that

$$\|\widetilde{S}_t - S_{th}\|_{L^2(\omega)} \leq C \max\{h_x, h_y\} \|\widetilde{S}_t\|_{W^{2,2}(\omega)} \leq C \max\{h_x, h_y\} \|\nabla \Pi J_h\|_{L^2(\omega)},$$

where the elliptic regularity on equation (3.25) is used. And Lemma 3.3 allows to bound the term $\|\nabla \Pi J_h\|_{L^2(\omega)}$. Moreover, from (3.11) and (3.25), we deduce that

$$\|\partial_t S - \widetilde{S}_t\|_{L^2(\omega)} \leq C \|J - \Pi J_h\|_{L^2(\omega)} \leq C(h_\theta^2 + \|f - \Pi f_h\|_{L^2(\omega \times [0,2\pi])}),$$

where we have used the error estimate given by the trapezoidal rule (3.23) to estimate $J - J_h$ for $f \in W^{2,2}(\omega \times [0, 2\pi])$. We conclude then that

$$\|\partial_t S - S_{th}\|_{L^2(\omega)} \leq \|\partial_t S - \widetilde{S}_t\|_{L^2(\omega)} + \|\widetilde{S}_t - S_{th}\|_{L^2(\omega)} \leq C(h_\theta^2 + \|f - \Pi f_h\|_{L^2} + \max\{h_x, h_y\}). \quad (3.26)$$

We introduce $\widetilde{S}$ weak solution of the elliptic problem

$$-\Delta \widetilde{S} + \widetilde{S} = \Pi \rho_h, \quad (3.27)$$

completed with Neumann boundary conditions. Therefore, we have that

$$\begin{aligned} \| \sup_{\alpha \in [0,2\pi]} |\mathbf{v}_\alpha \cdot \nabla_x S - \mathbf{v}_\alpha \cdot \nabla_x \widetilde{S}| \|_{L^2(\omega)} &\leq V \|S - \widetilde{S}\|_{W^{1,2}(\omega)} \leq C \|\rho - \Pi \rho_h\|_{L^2(\omega)} \\ &\leq C(h_\theta^2 + \|f - \Pi f_h\|_{L^2(\omega \times [0,2\pi])}), \end{aligned} \quad (3.28)$$

where we use the elliptic regularity for equation (3.27) and the error estimate for the trapezoidal rule (3.23). Moreover, $\Pi \rho_h$ belonging to $L^\infty(\omega) \hookrightarrow L^2(\omega)$, we have by elliptic regularity on (3.27) that $\widetilde{S} \in W^{2,2}(\omega)$. A Taylor expansion gives that for all $\mathbf{x} \in \omega$ and all $\alpha \in [0, 2\pi]$,

$$\widetilde{S}(t^n, \mathbf{x}) = \widetilde{S}(t^n, \mathbf{x} - \mathbf{v}_\alpha \Delta t) - \mathbf{v}_\alpha \cdot \nabla \widetilde{S}(t^n, \mathbf{x}) \Delta t + O_{L^2(\omega)}(\Delta t^2).$$

Hence, for all $\mathbf{x} \in \omega$

$$\begin{aligned} \| \sup_{\alpha \in [0,2\pi]} |\mathbf{v}_\alpha \cdot \nabla_x \widetilde{S}(t^n, \mathbf{x}) - \frac{1}{\Delta t}(S_h(t^n, \mathbf{x}) - \Pi S_h(t^n, \mathbf{x} - \mathbf{v}_\alpha \Delta t))| \|_{L^2_x(\omega)} \leq C \Delta t + \\ \frac{1}{\Delta t} \|\widetilde{S}(t^n, \mathbf{x}) - S_h(t^n, \mathbf{x})\|_{L^2_x(\omega)} + \frac{1}{\Delta t} \| \sup_{\alpha \in [0,2\pi]} |\widetilde{S}(t^n, \mathbf{x} - \mathbf{v}_\alpha \Delta t) - \Pi S_h(t^n, \mathbf{x} - \mathbf{v}_\alpha \Delta t)| \|_{L^2_x(\omega)}. \end{aligned}$$

Assumption 3.2 implies that the last two terms of the sum are equals. Since $S_h$ is obtained by solving equation (3.27) with conforming $\mathbb{P}^1$ finite elements, Proposition 3.1 implies that

$$\|\widetilde{S}(t^n, \cdot) - S_h(t^n, \cdot)\|_{L^2(\omega)} \leq C \max\{h_x, h_y\} \|\widetilde{S}\|_{W^{2,2}(\omega)}.$$

Therefore,

$$\| \sup_{\alpha \in [0,2\pi]} |\mathbf{v}_\alpha \cdot \nabla \widetilde{S}(t^n, \mathbf{x}) - \frac{1}{\Delta t}(S_h(t^n, \mathbf{x}) - \Pi S_h(t^n, \mathbf{x} - \mathbf{v}_\alpha \Delta t))| \|_{L^2(\omega)} \leq C(\Delta t + \frac{\max\{h_x, h_y\}}{\Delta t}). \quad (3.29)$$

Finally, injecting (3.26), (3.28), (3.29) in (3.24) and with Assumption 3.2, we obtain

$$\| \sup_{\alpha\in[0,2\pi]} |T(t^n,\cdot,\alpha) - T_h(t^n,\cdot,\alpha)|\|_{L^2(\omega)} \leq$$
$$\leq C(\Delta t + \max\{h_x,h_y\} + \frac{\max\{h_x,h_y\}}{\Delta t} + h_\theta^2 + \|f(t^n,\cdot,\cdot) - \Pi f_h(t^n,\cdot,\cdot)\|_{L^2(\omega\times[0,2\pi])}).$$

□

**Return to the proof of Theorem 3.4.** Since $\Pi$ is defined by its values at the nodes, we have that $\Pi(T_h f_h) = \Pi(\Pi T_h \Pi f_h)$. Then, for $k = 0,\dots,N_\theta - 1$,

$$|Tf(t^n,\mathbf{x}-\mathbf{v}_\theta\Delta t,\theta_k) - \Pi(T_h f_h)(t^n,\mathbf{x}-\mathbf{v}_\theta\Delta t,\theta_k)| \leq$$
$$|(1-\Pi)(Tf)(t^n,\mathbf{x}-\mathbf{v}_\theta\Delta t,\theta_k)| + |\Pi(Tf - \Pi T_h\Pi f_h)(t^n,\mathbf{x}-\mathbf{v}_\theta\Delta t,\theta_k)|.$$

Moreover,

$$|Tf - \Pi T_h \Pi f_h| \leq |T(f-\Pi f_h)| + |\Pi(f_h)(T - \Pi T_h)|. \tag{3.30}$$

From the definition of $T$ and with Lemma 3.3, we have $\|T\|_{L^\infty} \leq 1$ and $\|\Pi f_h\|_{L^\infty} \leq C$. From Assumption 3.2,

$$\begin{aligned}
&\| \sup_k |(\Pi(Tf) - \Pi T_h \Pi f_h)(t^n,\mathbf{x}-\mathbf{v}_\theta\Delta t,\theta_k)|\|_{L^2_{x,\theta}(\omega\times[0,2\pi])} \\
&\quad = 2\pi \| \sup_k |(Tf - \Pi T_h\Pi f_h)(t^n,\cdot,\theta_k)|\|_{L^2(\omega)} \\
&\quad \leq 2\pi \| \sup_k |(f-\Pi f_h)(t^n,\cdot,\theta_k)|\|_{L^2(\omega)} + C\| \sup_k |(T-\Pi T_h)(t^n,\cdot,\theta_k)|\|_{L^2(\omega)}.
\end{aligned}$$

And from (3.7) we have,

$$\| \sup_k |(1-\Pi)Tf(t,\cdot,\theta_k)|\|_{L^2(\omega)} \leq C\max\{h_x^2,h_y^2\}.$$

Thus by continuity of the application $\theta \mapsto (f-\Pi f_h)(t,\mathbf{x},\theta)$ we have from (3.30)

$$\| \sup_k |(Tf - \Pi(T_h f_h))(t^n,\cdot,\theta_k)|\|_{L^2(\omega)} \leq C(\epsilon^n + \max\{h_x^2,h_y^2\} + \| \sup_k |(T-\Pi T_h)(t^n,\cdot,\theta_k)|\|_{L^2(\omega)}),$$

where we use Lemma 3.3. It comes from the expression of $I_2$ (3.20) that

$$\begin{aligned}
\|I_2\|_{L^2(\omega)} &\leq 4\pi \| \sup_k |(Tf - \Pi(T_h f_h))(t^n,\cdot,\theta_k)|\|_{L^2(\omega)} \\
&\leq C(\Delta t + h^2 + \max\{h_x,h_y\} + \frac{\max\{h_x,h_y\}}{\Delta t} + \epsilon^n),
\end{aligned}$$

where we use Lemma 3.7. Moreover, Lemma 3.5 and 3.6 furnish an estimate on $(1-\Pi)I_1$ and $I_3$ in $L^2(\omega\times[0,2\pi])$ in inequality (3.22). It leads to

$$\epsilon^{n+1} \leq \epsilon^n + C_1\Delta t\left(\Delta t + h^2 + \frac{\max\{h_x,h_y\}}{\Delta t} + \max\{h_x,h_y\} + \epsilon^n\right).$$

A discrete Gronwall inequality enables us to get

$$\epsilon^n \leq \exp(C_1 t_0)\,\epsilon^0 + C_2\left(\Delta t + h^2 + \frac{\max\{h_x,h_y\}}{\Delta t} + \max\{h_x,h_y\}\right).$$

As $\epsilon^0$ is only a fixed interpolation error, we have $\epsilon^0 = 0$ and

$$\epsilon^n \leq C\left(\Delta t + h^2 + \frac{\max\{h_x, h_y\}}{\Delta t} + \max\{h_x, h_y\}\right).$$

□

This convergence result has been established under additional assumption which gives the invariance of all integrals on the computational domain along characteristics. Assumption 3.2 boils down to consider that the domain $\omega$ is very large with respect to the place where cells are. However the property of invariance of integrals along characteristics remains valid if we take into account boundary conditions at the boundary of the domain, provided that these boundary conditions are conservative (e.g. periodic boundary conditions, specular reflection conditions). The idea of the proof of Theorem 3.4 is the same but is much more technical since all integrals should be decomposed between a part for which characteristics meet the boundary and a part for which characteristics do not meet the boundary.

# 4 Numerical simulations

In this section, we present the numerical results obtained with the algorithm presented in Section 3. We are interested in the dynamics of the cells concentration for bacteria *E. Coli* in a Petri box. In this simulation we take the numerical values of [5] where the Petri box is strongly elongated. In fact, the authors are looking for traveling pulse at macroscopic scale due to the presence of nutrient. In their study, they observe the concentration of bacteria in a slice that moves along the Petri box. Here we do not consider nutrient and we want to study numerically the aggregation in a slice of the cells for such a Petri box. Then we take $\omega = [0, L_x] \times [0, \ell_y]$ with $L_x = 10^{-2}\, m$ and $\ell_y = 10^{-3}\, m$. Moreover this very elongated device allows us to avoid the influence of the left and right boundary. Bacteria are modelled by spheres of radius $1\,\mu m$. Their initial density is assumed to be $n_0 = 10^8$ cells per $cm^{-3}$. Each individual cell has a constant speed $V = 20\,\mu m.s^{-1}$ during the *run* phase.

## 4.1 Numerical results

The Keller-Segel model [28] was originally derived to describe aggregation of cells. Microscopic models presented here allow to incorporate additional informations during the motion and therefore to obtain an accurate description of the dynamics of the cells concentration. We present numerical simulations of model (1.5) using the algorithm described in Section 3 with a Hermite spline interpolation method.

We assume that cells are initially concentrated in a slice of the device :

$$f^0(x, y, \theta) = n_0 \frac{\sqrt{C_x}}{\pi} \exp(-C_x(x - 0.5L_x)^2), \qquad \text{with} \quad C_x \gg 1. \tag{4.1}$$

In this simulation, we take $N_x = 120$, $N_y = 20$ and $N_\theta = 52$. The time step is chosen $dt = 4.10^{-2}$ and the constant $C_x = 2\,.10^5$. For such initial data and since for specular reflection the evolution is invariant in the $y$-direction, we only represent in Figure 1 the dynamics of the

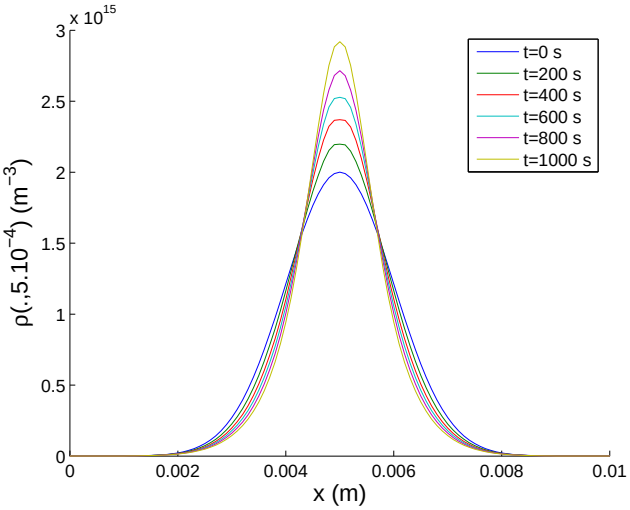


Figure 1: Dynamics of the density $\rho(t, x, \ell_y/2)$ for different times. One can observe concentration of cells in the center $x = L_x/2$.

density $\rho$ in a horizontal section $y = \ell_y/2$ of the device. As time becomes longer, we notice aggregation of cells in the center $x = L_x/2$.

To illustrate the dynamics of the density in the Petri dish, we non-dimensionalize the system (1.1) by introducing the dimensionless quantities

$$x = x_0\overline{x}, \qquad t = t_0\overline{t}, \qquad v = v_0\overline{v},$$
$$S(t,x) = S_0\overline{S}(\overline{t},\overline{x}), \qquad f(t,x,v) = f_0\overline{f}(\overline{t},\overline{x},\overline{v}), \qquad \phi(z) = \phi_0\overline{\phi}(z).$$

$\phi_0$ is the typical value for the size of the turning kernel, $v_0 = V$ is the typical speed, $x_0 = L_x$ is the characteristic length of the device and the typical time is defined by $t_0 = x_0/v_0$. Using the same arguments than in [16], the dimensionless system is (dropping the bars)

$$\begin{aligned} \partial_t f + v\cdot\nabla_x f &= \mu\left(\int_{\mathbb{S}_V}\phi(\partial_t S + v'\cdot\nabla_x S)f(v')\,dv' - 2\pi\phi(\partial_t S + v\cdot\nabla_x S)f(v)\right), \\ -\Delta S + S &= \rho, \end{aligned} \tag{4.2}$$

where we set $\mu = \dfrac{\phi_0 x_0}{v_0}$. With the numerical values used here, we have $\phi_0 = 1$ and obtain $\mu = 5\,10^3$. Here $\mu \gg 1$, then the solutions of the kinetic model are not far from solutions of the macroscopic model obtained thanks to the hydrodynamic limit $\mu^{-1} \to 0$. The rigorous derivation of the hydrodynamic limit for prescribed smooth chemoattractant density is carried out in ref. [16]. We recall that the hydrodynamic limit is given by

$$\begin{aligned} &\partial_t\rho + \mathrm{div}_x\left(\rho\,\chi(\partial_t S, |\nabla_x S|)\nabla_x S\right) = 0, \\ &-\Delta S + S = \rho, \end{aligned} \tag{4.3}$$

where $\chi(\partial_t S, |\nabla_x S|)$ is the chemotactic sensitivity. In the case $\alpha = 0$ in the definition of $\phi$ (1.4), this chemotactic sensitivity can be computed explicitly (see [16]). We find

$$\chi(\partial_t S, |\nabla_x S|) = \frac{6V}{2\pi - 3/2\arccos(\partial_t S/(V|\nabla_x S|))}\sqrt{1 - \left(\frac{\partial_t S}{V|\nabla_x S|}\right)^2}\,\frac{1}{|\nabla_x S|},$$

if $|\partial_t S/(V\nabla_x S)| < 1$, and $\chi(\partial_t S, |\nabla_x S|) = 0$ if $|\partial_t S/(V\nabla_x S)| \geq 1$ or $\nabla_x S = 0$. In [16], the authors implement a numerical simulation of this macroscopic model allowing to observe aggregation for Dictyostelium Discoideum where a very simple model for the production of cAMP is used. We recover here this dynamics.

## 4.2 Influence of the $\partial_t S$ term

In several papers [8, 11], the kinetic system presented in (1.5) is studied assuming that the turning operator does not depend on the partial derivative of $S$ with respect to time. In [6], a critical mass phenomenon occurs in a kinetic model and the solutions converge in finite time to a Dirac under the assumption that the turning kernel grows linearly with $\nabla_x S$. In this section we present numerical simulations when the turning kernel only depends on the spatial gradient of the chemoattractant concentration $S$. The system considered is then (1.5) where we drop the term $\partial_t S$ :

$$\begin{cases} \partial_t f + v \cdot \nabla_x f = \displaystyle\int_{v' \in \mathcal{V}} \phi(v' \nabla_x S) f(v')\, dv' - 2\pi \phi(v \nabla_x S) f(v), \\ f(0, x, v) = f^0(x, v), \\ -\Delta S + S = \rho(t, x) := \displaystyle\int_{v \in \mathcal{V}} f(t, x, v)\, dv, \end{cases} \tag{4.4}$$

It boils down to assume that cells are able to evaluate the gradient of chemoattractant at their position. Actually when cells are big enough and have sensors along their body like slime mold Dictyostelium Discoideum [19], they can sense the chemoattractant concentration along their body. For such amoeba, the use of this system is relevant. Here it can be understood as a model simplification.

Figure 2 on the left represents the dynamics in the section $y = \ell_y/2$ of the density obtained by solving the model with the algorithm described in Section 3 using a Hermite spline interpolation method. We observe spurious oscillations near the maximum of the density. Whereas when we apply the same algorithm with a linear interpolation method the oscillations disappear (Figure 2 on the right). These artificial oscillations are known as Runge phenomenon.

We observe that the aggregation phenomenon is stronger than in previous subsection. In fact the maximum value of $\rho$ for $t = 125\, s$ in this case is greater than $10^{16}\, m^{-3}$ whereas in Figure 1 even for $t = 1000\, s$ the maximum is smaller than $3.\, 10^{15}\, m^{-3}$. Moreover the dynamics of $\rho$ does not seem to be smooth in the vicinity the position $x = L_x/2$. Comparing with Figure 1, the aggregation is faster and less regular than when we use the term $\partial_t S$ for the computation of $T$. This large and rapid variation of $\rho$ in the vicinity of the maximum is surely responsible of oscillations that appear with a high order interpolation method in this case whereas no Runge phenomenon is noticed in Figure 1.

This simulation seems to indicate that the solution blows up as a Dirac in the center of the device. A simple argument in 1D confirms this observation. In fact, the dimensionless 1D version of (4.4) is written for all $x \in [0, L]$ and $v \in \{-V, V\}$

$$\partial_t f + v \partial_x f = \mu(\phi(-v \partial_x S) f(-v) - \phi(v \partial_x S) f(v)),$$

with $\mu \gg 1$. When $\mu^{-1} \to 0$, the equilibrium is obtained for

$$f(-v) = \frac{\phi(-v \partial_x S)}{\phi(v \partial_x S)} f(v). \tag{4.5}$$

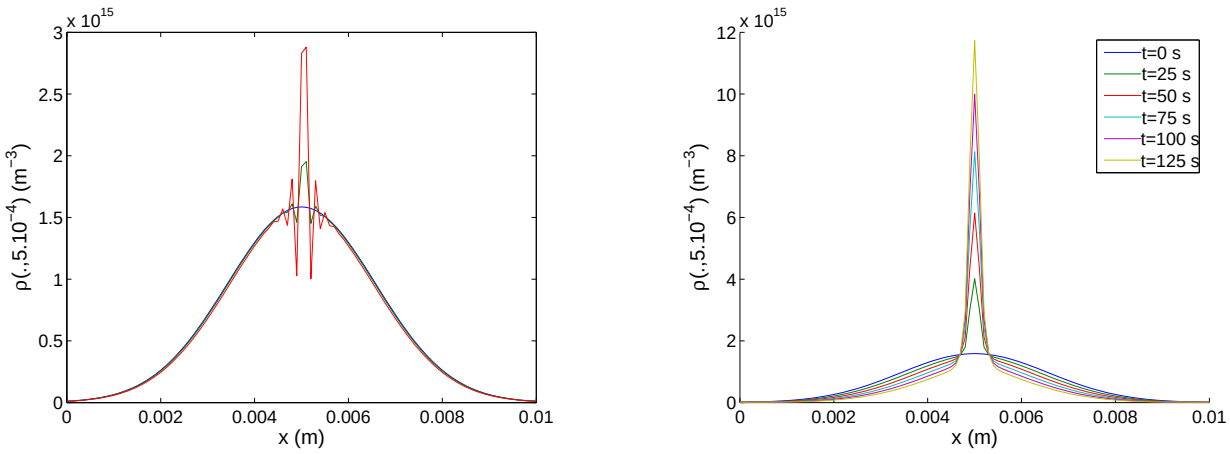


Figure 2: Dynamics of the density $\rho(t, x, \ell_y/2)$ when the turning kernel depends only on $\partial_x S$ (4.4). On the left we use a Hermite spline interpolation method : spurious oscillations appear (Runge phenomenon). On the right a linear interpolation method is implemented.

Summing the one dimensional kinetic equations for $v = V$ and $v = -V$, we obtain the equation for the first moment :

$$\partial_t(f(V) + f(-V)) + V\partial_x(f(V) - f(-V)) = 0. \tag{4.6}$$

Moreover, assuming that $f$ is at equilibrium (4.5) we deduce that

$$f(V) - f(-V) = \frac{\phi(-V\partial_x S) - \phi(V\partial_x S)}{\phi(-V\partial_x S) + \phi(V\partial_x S)}(f(V) + f(-V))$$

The density at equilibrium is defined by $\rho := f(V) + f(-V)$. With (4.6) we finally obtain the 1D version of the hydrodynamic model (4.3) without $\partial_t S$ :

$$\partial_t \rho + \partial_x(a(\partial_x S)\rho) = 0, \tag{4.7}$$

where

$$a(\partial_x S) = V\,\frac{\phi(-V\partial_x S) - \phi(V\partial_x S)}{\phi(-V\partial_x S) + \phi(V\partial_x S)}. \tag{4.8}$$

We can approximate the model by assuming that $\alpha$ in (1.4) is small compared to the values of the chemoattractant concentration gradient such that $\phi(z) = 1/4$ for $z > 0$ and $\phi(z) = 1$ for $z < 0$. In this case, we deduce from (4.8) that

$$a(\partial_x S) = \frac{3}{5}V \text{ sign } (\partial_x S), \tag{4.9}$$

where the function sign is defined by

$$\text{sign } (z) = 1 \text{ for } z > 0\,;\ -1 \text{ for } z < 0\,;\ 0 \text{ for } z = 0.$$

This system is completed with the elliptic equation for $S$ :

$$-\partial_{xx} S + S = \rho.$$

We can prove that with our initial guess $f^0$ (4.1) the function $S$ is increasing for $x < 0.5L_x$, decreasing for $x > 0.5L_x$. Therefore, sign $(\partial_x S) =$ sign $(x - 0.5L_x)$ and equation (4.7) becomes

$$\partial_t \rho + \partial_x(\frac{3}{5}V \text{ sign } (x - 0.5L_x)\rho) = 0.$$

It is well-known that the solution $\rho$ of this hyperbolic system becomes instantaneously a Dirac at $x = 0.5L_x$ (see e.g. [36]).

In the case studied in the previous subsection where the term $\partial_t S$ is not neglected, the hydrodynamic limit leads to

$$\partial_t \rho + \partial_x(a(\partial_t S, \partial_x S)\rho) = 0,$$

where

$$a(\partial_t S, \partial_x S) = V \frac{\phi(\partial_t S - V\partial_x S) - \phi(\partial_t S + V\partial_x S)}{\phi(\partial_t S - V\partial_x S) + \phi(\partial_t S + V\partial_x S)}. \tag{4.10}$$

Figure 1 seems to show that the presence of the term $\partial_t S$ has a *regularization* effect. The rigorous mathematical analysis of these phenomena is a work in progress.

## 4.3 Locus of aggregation

Another interesting question is the determination of the aggregation locus. In the previous case when $f^0$ is given in (4.1) and is symmetric, the aggregation takes place in the center of the device where the concentration is initially maximal. However, in Figure 3, we represent the dynamics of the density when the initial data is not symmetric :

$$f^0(x, y, \theta) = \begin{cases} n_0 \dfrac{\sqrt{C_x}}{\pi} \exp(-C_x(x - 0.5L_x)^2), & \text{for } x \in [L_x/2, L_x], \\ n_0 \dfrac{\sqrt{C_x}}{\pi} \exp(-0.5C_x(x - 0.5L_x)^2), & \text{for } x \in [0, L_x/2]. \end{cases}$$

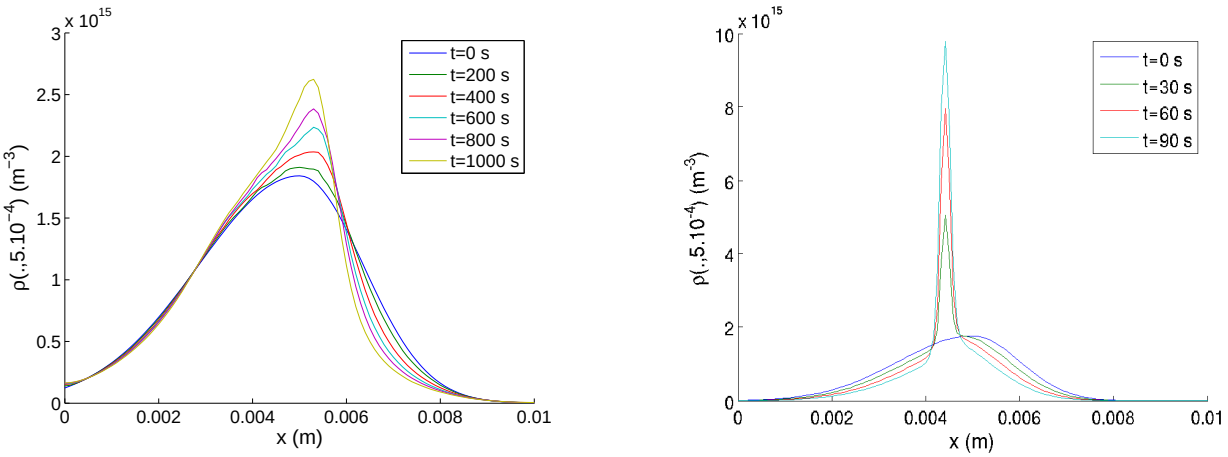


Figure 3: Dynamics of the density $\rho(t, x, \ell_y/2)$ when the initial concentration is a smooth function but not symmetric. Left : with the term $\partial_t S$ in the definition of the turning kernel (1.5). Right : without $\partial_t S$ (4.4).

Figure 3 left represents dynamics of the density $\rho(t, x, \ell_y/2)$ when the turning kernel depends of the temporal derivative of the chemical signal $\partial_t S$ as in (1.5). Figure 3 right represents

evolution of $\rho$ when $\partial_t S$ is dropped in the definition of the turning kernel (4.4). We observe that the aggregation locus is not the same with and without $\partial_t S$. As noticed previously, the behaviour of solutions seems to be more regular for model (1.5) than with (4.4).

For model (4.4) when the term $\partial_t S$ is dropped in the definition of the turning kernel (Figure 3 right) the place where aggregation occurs seems to be invariant and fixed. It is readily seen in this case that the points where accumulation occurs for the one dimensional problem (4.7)–(4.9) are the points $x_0$ for which $\partial_x S(x_0) = 0$ and is maximal. In fact, the characteristics for the conservation law (4.7) converge and cross at these points. When the temporal derivative of the chemoattractant is not neglected, a careful study of the expression (4.10) is needed to determine the points where aggregation occurs. In Figure 3 left, the locus of the maximum of $\rho$ is not invariant.

We consider now the case when the density of cells is not invariant with respect to $y$. We assume for instance that cells are initially concentrated in the center of the device :

$$f^0(x, y, \theta) = n_0 \frac{\sqrt{20} C_x}{2\pi} \exp(-C_x((x - 0.5L_x)^2 + 20(y - 0.5\ell_y)^2)).$$

For this simulation, we take $N_y = 40$ and $C_x = 10^6$. Figure 4 presents the evolution of the density of cells in the device. We observe an evolution in two steps. Firstly, cells diffuse in the $y$ direction. After $2250\, s$, when the density becomes invariant with respect to $y$, aggregation phenomenon involves in a slice in the center of the device.

On the one hand, this dynamics is not comparable to the one observed without the dependence on $\partial_t S$ of the turning kernel (4.4). Actually, we notice in Figure 5 that for model (4.4) the blow up occurs in the center of the device. On the other hand, let us consider a square domain $L_x = \ell_y = 7.\,10^{-3}$ m and spherically symmetric initial data

$$f^0(x, y, \theta) = n_0 \frac{C_x}{2\pi} \exp(-C_x((x - 0.5L_x)^2 + (y - 0.5\ell_y)^2)).$$

We observe in Figure 6 that bacterias concentrate in the center of the device. We conclude then that the behaviour observed in Figure 4 is due to the particular domain that we take which is very thin in the $y$-direction. In fact, due to specular reflection at the boundary, bacterias on the slice $x = 0.5L_x$ close to the boundary that swim in an unfavorable direction (i.e. for which the gradient of the chemoattractant decreases), reflect to the top or bottom boundary. After a reflection they swim in a favourable direction (i.e. for which the gradient of the chemoattractant along their paths increases). Since the device is very elongated, cells are initially close to the top and the bottom boundary; this is the reason why we first notice a diffusion in the $y$ direction.

# 5 Conclusion

A kinetic model describing chemotaxis for a population of bacteria has been presented in (1.5). This model has been previously introduced in ref. [16] where its hydrodynamic limit was derived. It incorporates the ability of cells to assess temporal changes of the chemoattractant concentration as well as its spatial variations. In this work, we are interested in obtaining a numerical simulation of this kinetic model. We proved rigorously in Theorem 2.2 existence and uniqueness of solutions for this model. Then a semi-Lagrangian method has been implemented to obtain numerical simulations of this well-posed problem in Section 4.

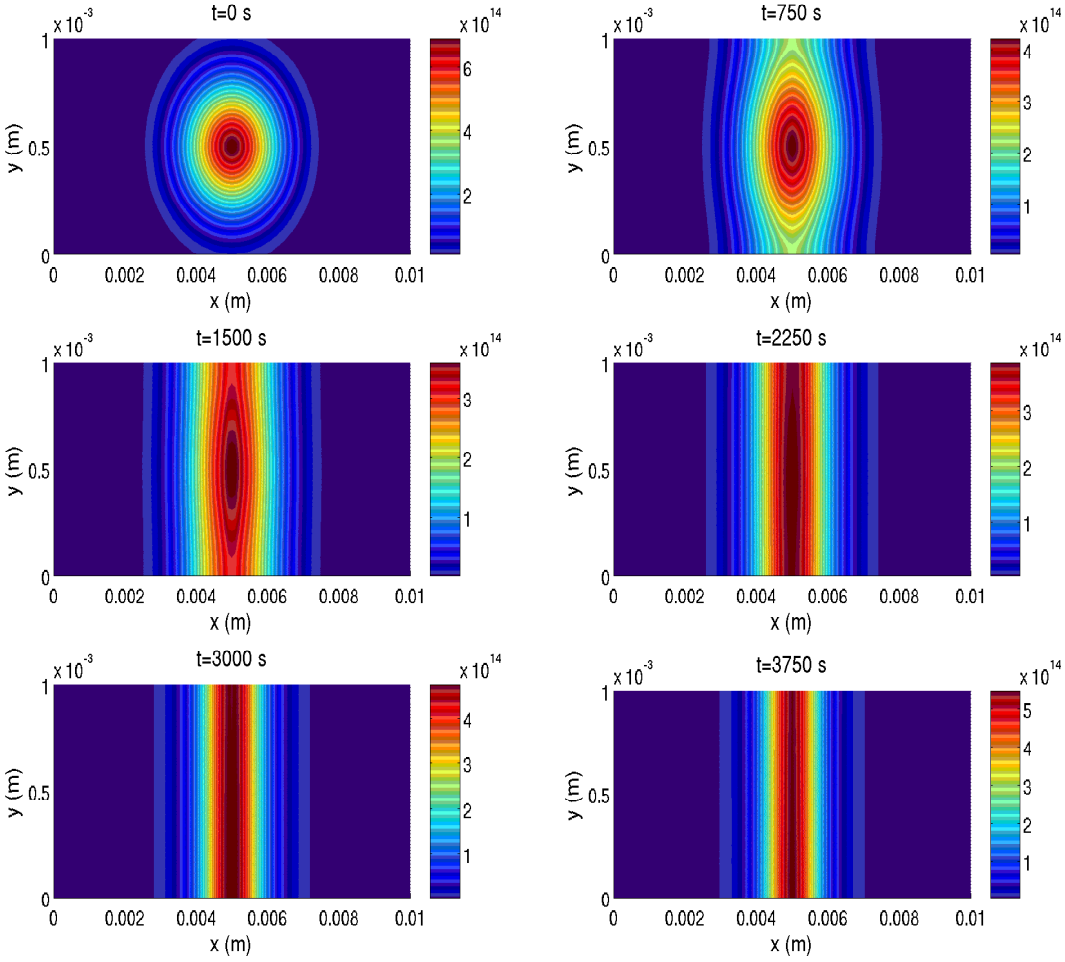


Figure 4: Dynamics of the density $\rho$ of cells in the device for model (1.5).

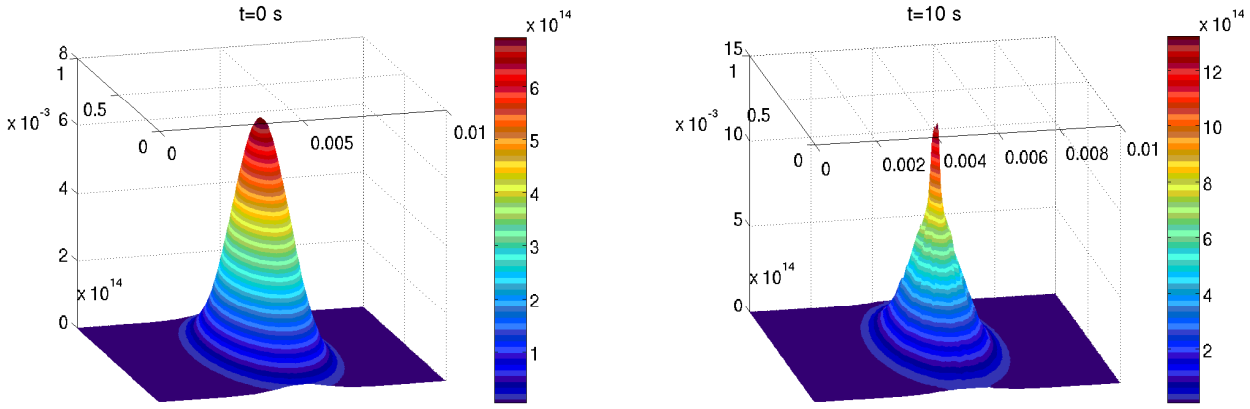


Figure 5: Dynamics of the density $\rho$ of cells in the device without the $\partial_t S$ dependence of the turning kernel (4.4) when the concentration is initially maximal in the center of the device.

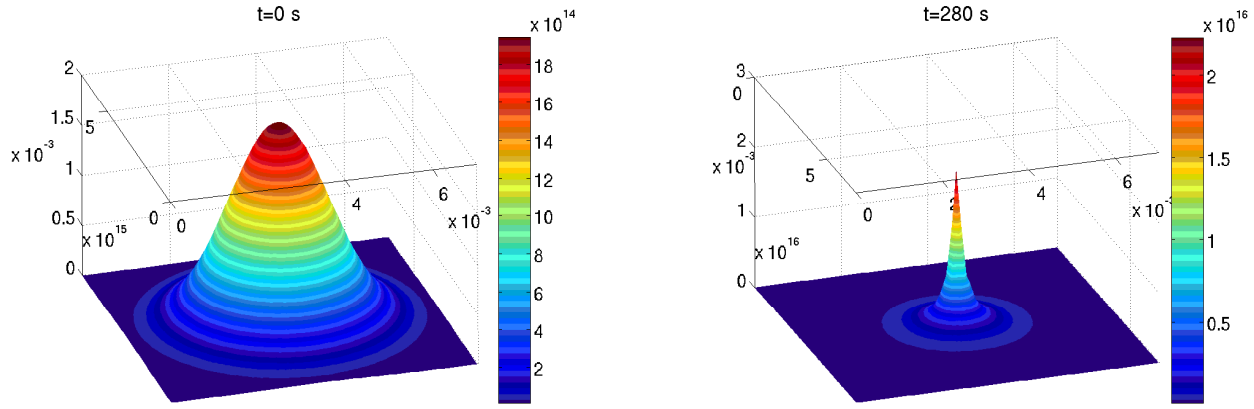


Figure 6: Dynamics of the density $\rho$ of cells for a square domain with the $\partial_t S$ dependence of the turning kernel when the concentration is initially maximal in the center of the device.

We have noticed in this simulation aggregation of cells in some place of the device. This aggregation phenomenon was observed in experiments and mathematical study of this phenomenon was the motivation of the work of Keller and Segel [28]. Some numerical simulations of macroscopic models describing chemotaxis have been obtained (see e.g. [10, 20, 21, 16, 24, 37]) but not at microscopic level which is the aim of this work.

We have tested two expressions of the turning kernel which is taken depending on the temporal derivative of the chemical signal or not. A first observation is the fact that the presence of the term $\partial_t S$ in the definition of the $T$ seems to smooth solutions and to slow down the aggregation phenomena. This phenomena was expected since in the case 'without $\partial_t S$' cells are able to estimate instantly the gradient of the chemical and to decide instantly either to change direction or not. In the case 'with $\partial_t S$' cells must swim (at least during one numerical time step) to sense the chemical gradient. Moreover the place where aggregation occurs is not exactly the same for both models in some situation. A rigorous explanation of these phenomena for these mathematical models is at our knowledge still an open question.

Furthermore, the numerical simulation of model (1.5) implemented in this article shows the blow-up along lines while for the Keller-Segel model the blow-up is always point-wise [10, 20, 24, 29, 37, 38]. It is observed in [20, 37] that due to instabilities the blow-up peak usually moves to a corner of the computational domain. In [29] the mass concentrates in some particular points of the boundary that can collides to form isolated peaks in the boundary of domain. In [24], the authors concentrate on capturing the correct blow-up dynamics by using a particle method : cells aggregate in two singularities that collide to form one single heavy particle carrying almost all of the mass while diffusion occurs in the rest of the domain. However, in the numerical test presented in this paper, one can observe blow-up profiles that are not point-wise and that can be located inside the domain. Moreover, blow up profiles along lines seems to be stable (see Figure 4).

Finally, this study leads to the question of deriving macroscopic model from this kinetic system. When the time derivative is not taken into account in the expression of the turning kernel, we refer to [21] when a hierarchy of models is presented. Including the time derivative of the chemical implies that all coefficients depending on $S$ at the macroscopic level depends on $\partial_t S$ too, such as in model (4.3). However, this term represents the dynamics of the gradient

of the chemoattractant along the trajectories of the cells. At macroscopic level, it has no meaning since we do not consider the motion of individual cells. From a mathematical point of view, we can use (2.2) to have an expression of $\partial_t S$ with respect to the flux of cells which is a macroscopic quantity. An other idea following [16] is to consider an evolution equation for the chemoattractant density, even if the time scaling of this equation is very fast compared to the cells dynamics.

**Acknowledgement.** The author thanks warmly Benoît Perthame for its valuable comments, his help and his support during this work.

# References

[1] W. Alt, *Biased random walk models for chemotaxis and related diffusion approximations*, J. Math. Biol. **9**, 147–177 (1980).

[2] R. Belaouar, N. Crouseilles, P. Degond, E. Sonnendrücker, *An asymptotically stable semi-Lagrangian scheme in the quasi-neutral limit*, preprint (2007).

[3] N. Besse, *Convergence of a semi-Lagrangian scheme for the one dimensional Vlasov-Poisson system*, SIAM J. Numer. Anal. **42**, no 1, 350–382 (2004).

[4] C.K. Birsdall, A.B. Langdon, *Plasma physics via computer simulation*, McGraw-Hill, New York, 1985.

[5] N. Bournaveas, A. Buguin, V. Calvez, B. Perthame, J. Saragosti, P. Silberzan, *Mathematical description of bacterial traveling pulses*, arXiv:0912.1792v1.

[6] N. Bournaveas, V. Calvez, *Critical mass phenomenon for a chemotaxis kinetic model with spherically symmetric initial data*, arXiv:0901.0503.

[7] N. Bournaveas, V. Calvez, *Global existence for the kinetic chemotaxis model without pointwise memory effects, and including internal variables*, Kinet. Relat. Models **1**, no 1, 29–48 (2008).

[8] N. Bournaveas, V. Calvez, S. Gutièrrez, B. Perthame *Global existence for a kinetic model of chemotaxis via dispersion and Strichartz estimates*, Comm. P.D.E. **33**, 79–95 (2008).

[9] J.P. Boris, D.L. Book, *solution of continuity equations by the method of flux-corrected transport*, J. Comput. Phys. **20**, 397–431 (1976).

[10] C.J. Budd, R. Carretero-González, R.D. Russell, *Precise computations of chemotactic collapse using moving mesh methods*, J. Comput. Phys. **202** 2, 463–487.

[11] F.A.C.C. Chalub, P.A. Markowich, B. Perthame, C. Schmeiser, *Kinetic models for chemotaxis and their drift-diffusion limits*, Monatsh. Math. **142**, 123–141 (2004).

[12] C.Z. Cheng, G. Knorr, *The integration of the Vlasov equation in configuration space*, J. Comput. Phys. **22**, 330–351 (1976).

[13] P.G. Ciarlet, *Basic error estimates for elliptic problems*, in Handbook of Numerical Analysis, Finite element methods (Part 1), Vol. II, P.G. Ciarlet and J.L. Lions, eds., North-Holland, New-York, 1991, 17–351.

[14] N. Crouseilles, F. Filbet, *Numerical approximation of collisional plasma by high order methods*, J. Comp. Phys. **201**, 2 (2004) 546–572.

[15] N. Crouseilles, G. Latu, E. Sonnendrücker, *Hermite spline interpolation on patches for parallely solving the Vlasov-Poisson equation*, Int. J. Appl. Math. Comput. Sc. **17**, 3 (2007) 101–115.

[16] Y. Dolak, C. Schmeiser, *Kinetic models for chemotaxis : Hydrodynamic limits and spatio-temporal mechanisms*, J. Math. Biol. **51**, 595–615 (2005).

[17] R. Erban, H.J. Hwang, *Global existence results for complex hyperbolic models of bacterial chemotaxis*, Disc. Cont. Dyn. Systems-Series B **6**, no 6, 1239–1260 (2006).

[18] R. Erban, H.G. Othmer, *From individual to collective behavior in bacterial chemotaxis*, SIAM J. Appl. Math. **65** (2004/05), no 2, 361–391

[19] R. Erban, H.G. Othmer, *Taxis equations for amoeboid cells*, J. Math. Biol. **54**, no 6, 847–885 (2004).

[20] F. Filbet, *A finite volume scheme for the Patlak-Keller-Segel chemotaxis model*, Numer. Math. **104** (2006), no 4, 457–488.

[21] F. Filbet, Ph. Laurençot, B. Perthame, *Derivation of hyperbolic models for chemosensitive movement*, J. Math. Biol. **50**, 189–207 (2005).

[22] F. Filbet, E. Sonnendrücker, P. Bertrand, *Conservative numerical schemes for the Vlasov equation*, J. Comput. Phys. **172** (2001) 166–187.

[23] F. Filbet, E. Sonnendrücker, *Comparison of Eulerian Solver*, Comput. Phys. Commun. **151** (2003) 247–266.

[24] J. Haskovec, C. Schmeiser, *Stochastic Particle Approximation for measure valued solutions of the 2D Keller-Segel system*, J. Stat. Phys. **135** 1, (2009), 133–151.

[25] T. Hillen, K.J. Painter, *A user's guide to PDE models for chemotaxis*, J. Math. Biol. **58** (2009), no 1-2, 183–217.

[26] D. Horstmann, *From 1970 until present : the Keller-Segel model in chemotaxis and its consequences*, Jahrsber. Dtsch. Math.-Ver. Vol. 105, 103-165 (2003).

[27] H.J. Hwang, K. Kang, A. Stevens, *Global solutions of nonlinear transport equations for chemosensitive movement*, SIAM J. Math. Anal. **36** 4, 1177–1199 (2005).

[28] E.F. Keller, L.A. Segel, *Initiation of slime mold aggregation viewed as instability*, J. Theor. Biol. **26**, 399–415 (1970).

[29] A. Marrocco, *2D simulation of chemotaxis bacteria aggregation*, ESAIM M2AN **37** (4), 617–630 (2003).

[30] N. Mittal, E.O. Budrene, M.P. Brenner, A. van Oudenaarden *Motility of Escherichia coli cells in clusters formed by chemotactic aggregation*, PNAS, November 2003, vol 100, no 23, 13259–13263.

[31] H.G. Othmer, S.R. Dunbar, W. Alt, *Models of dispersal in biological systems*, J. Math. Biol. **26**, 263–298 (1988).

[32] H.G. Othmer, T. Hillen, *The diffuion limit of transport equations. II. Chemotaxis equations*, SIAM J. Appl. Math. **62**, 1222–1250 (2002).

[33] H.G. Othmer, A. Stevens, *Aggregation, blowup, and collapse : the ABCs of taxis in reinforced random walks*, SIAM J. Appl. Math. **57**, 1044–1081 (1997).

[34] C.S. Patlak, *Random walk with persistence and external bias*, Bull. Math. Biophys. **15** (1953), 263–298.

[35] B. Perthame, *PDE models for chemotactic movements : parabolic, hyperbolic and kinetic*, Appl. Math. **49** 6, 539–564 (2004).

[36] F. Poupaud, M. Rascle, *Measure solutions to the linear multi-dimensional transport equation with non-smooth coefficients*, Comm. Partial Differential Equations **22** (1997), no 1-2, 337–358.

[37] N. Saito, *Conservative upwind finite element method for a simplified Keller-Segel system modelling chemotaxis*, IMA J. Num. Analysis **27** 2 (2007), 332–365.

[38] N. Saito, T. Suzuki, *Notes on finite difference schemes to a parabolic-elliptic system modelling chemotaxis*, Applied Mathematics and Computation **171** 1, (2005), 72–90.

[39] E. Sonnendrücker, J. Roche, P. Bertrand, A. Ghizzo, *The semi-Lagrangian method for the numerical resolution of the Vlasov equation*, J. Comput. Phys. **149** (1999) 201–220.

[40] E. Stevens, *The derivation of chemotaxis equations as limit dynamics of moderately interacting stochastic many particle systems*, SIAM J. Appl. Math. **61**, 183–212 (2000).

[41] M.J. Tindall, S.L. Porter, P.K. Maini, G. Gaglia, J.P. Armitage, *Overview of mathematical approaches used to model bacterial chemotaxis. I. The single cell.* Bull. Math. Biol. **70** (2008), no 6, 1525–1569.